

An Investigation of Therapeutic Potential of Plant-Made Cholera Toxin B Subunit, an Orally Active Anti-inflammatory Protein, in a Mouse Model of Acute Colitis

Bailey A. Nelson^{1,3}, Joshua M. Royal^{2,3}, Keegan Baldauf^{1,3}, Calvin Kouokam³, and Nobuyuki Matoba^{1,2,3}

¹Department of Pharmacology and Toxicology and ²James Graham Brown Cancer Center

University of Louisville School of Medicine, Louisville, KY 40202, and ³The Owensboro Cancer Research Program, Owensboro, KY 42303

Introduction

Cholera toxin B subunit (CTB)

- Non-toxic subunit of cholera holotoxin; 55kDa in size
- A component in an internationally licensed oral cholera vaccine (Dukoral®)
- Induces strong anti-inflammatory response
 - *In vivo*, CTB suppressed pathogenic immune responses associated with allergy and Crohn's disease^{2,5}

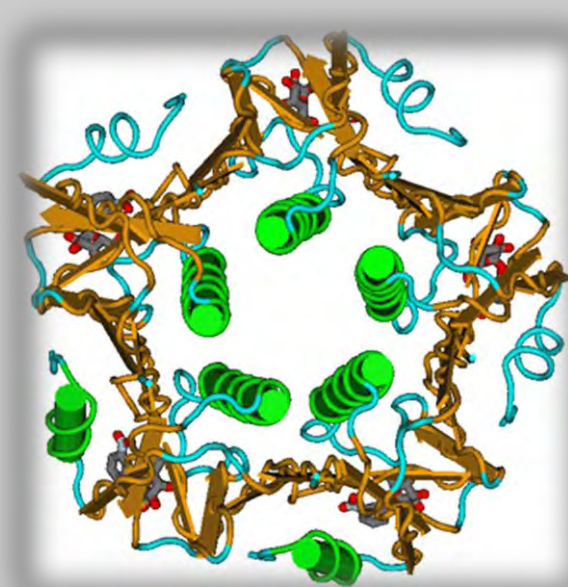


Figure 1. Pentamer structure CTB depicted with Cn3D software.

Robust Plant Production System of CTB

- Our group has generated a variant of recombinant CTB (CTBp) in *Nicotiana benthamiana* plants³
- Remarkably high and uniform expression of CTBp in 5 days
 - Demonstrated GM1 ganglioside binding affinity and oral immunogenicity equivalent to the original Dukoral vaccine antigen.

Mouse Model of Inflammatory Bowel Disease (IBD)

- CTB has been shown to protect against inflammation^{1,4}
- The present study utilized a model of ulcerative colitis (UC) in mice
 - Dextran Sodium Sulfate (DSS) disrupts tight junctions in intestinal epithelium
 - induces a similar response in mice as human UC, which is T helper 2 mediated

Previous Results¹

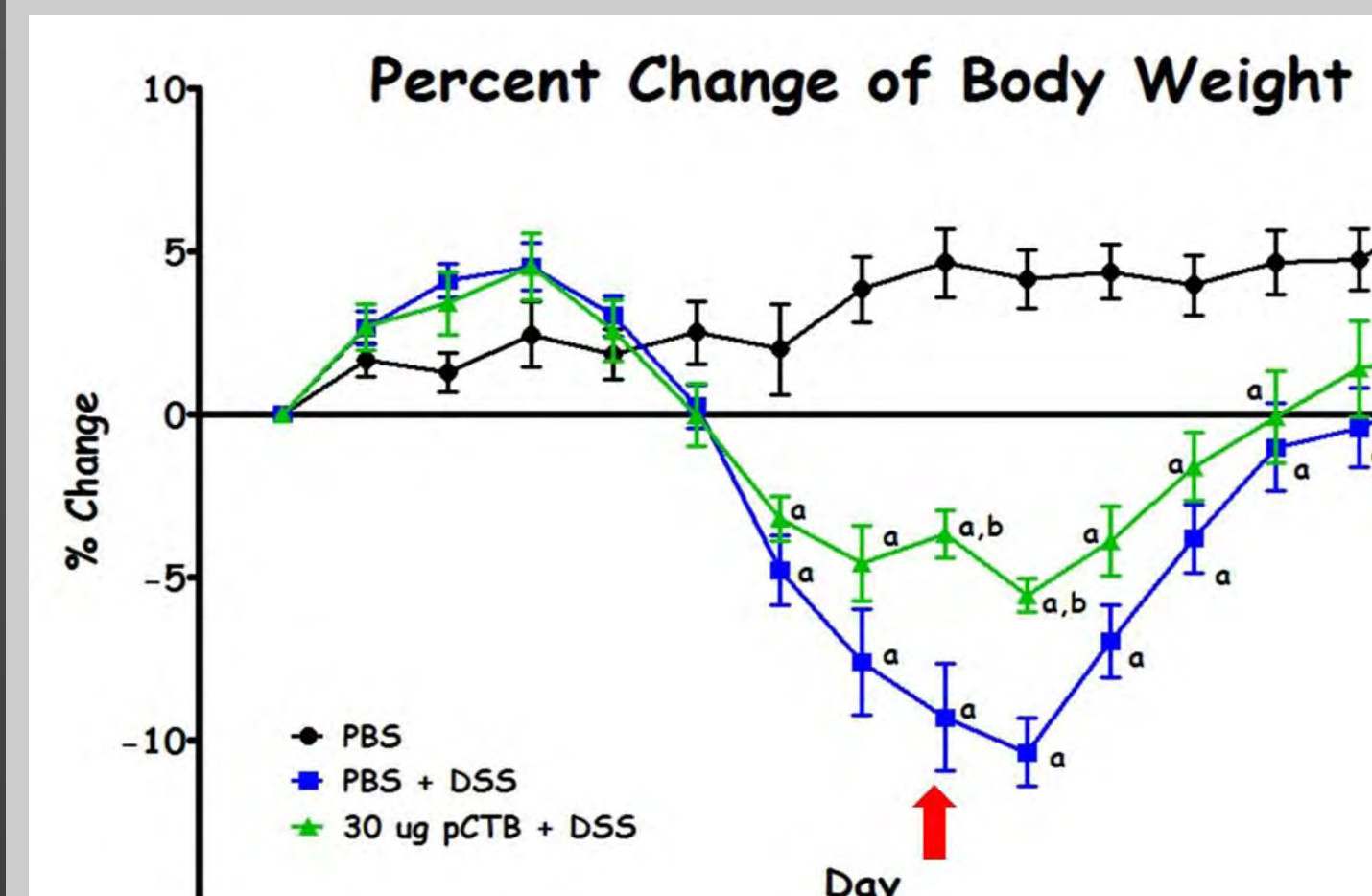


Figure 2. Percent body weight change. Mice were exposed to 4% DSS for 8 days and allowed to recover for 6 days- red arrows. CTBp (30µg) was orally administered 2 weeks prior to and the day of the initiation of DSS exposure.

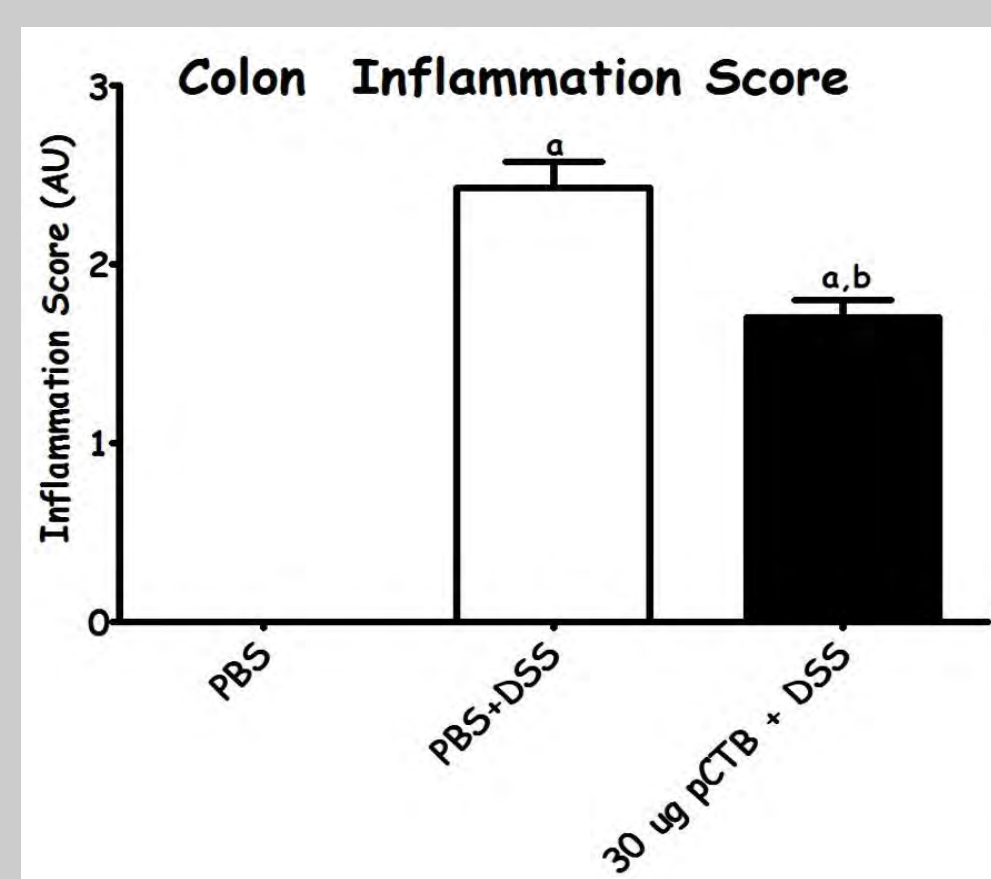


Figure 3. Recovery Inflammation Scoring. Inflammation scoring of H&E sections. a= p<0.05 compared to PBS. b=p<0.05 compared to PBS+DSS. One-way ANOVA with Bonferroi's post-tests (GraphPad Prism 5 software).

Summary of Previous Studies

- CTBp given via oral gavage prior to DSS exposure protected mice from weight loss and blunted inflammation in the colon.
- CTBp altered colon gene expression profile; reduced pro-inflammatory cytokines and increased collagens.

Aims

- Use the DSS acute colitis mouse model to:
 - Analyze effectiveness of CTBp dosed during DSS exposure
 - Compare with the anti-TNFα antibody Infliximab (Remicade®)

Results



Figure 4. Percent change of body weight. Mice were exposed to 3% DSS for 7 days and allowed to recover for 2 days then sacrificed. No difference was observed between groups (two-way ANOVA).

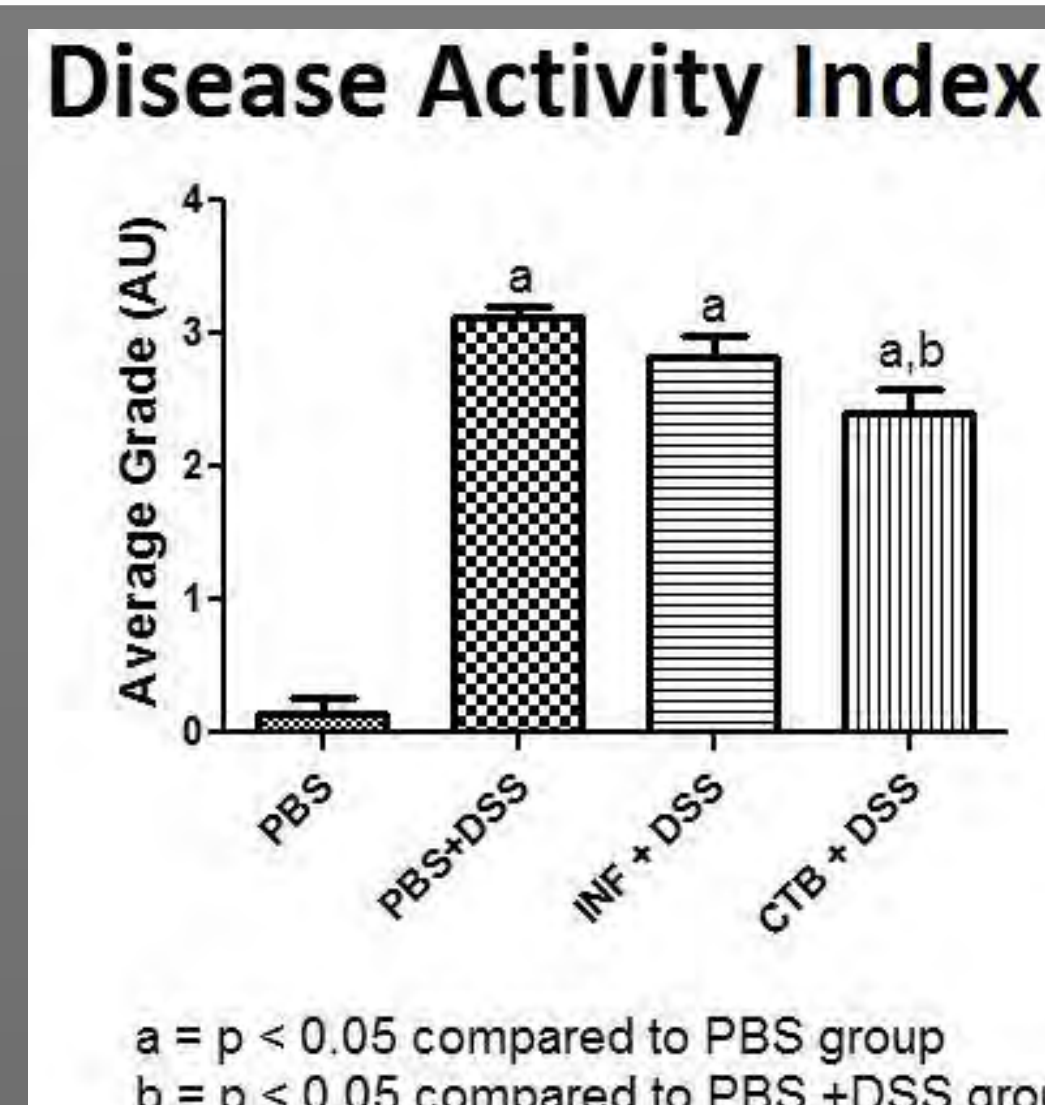


Figure 5. Disease Activity Index (DAI). DAI scores were determined Day 9. One-way ANOVA with Bonferroi post-tests was performed: a = p<0.05 compared to PBS, b = p<0.05 compared to PBS+DSS

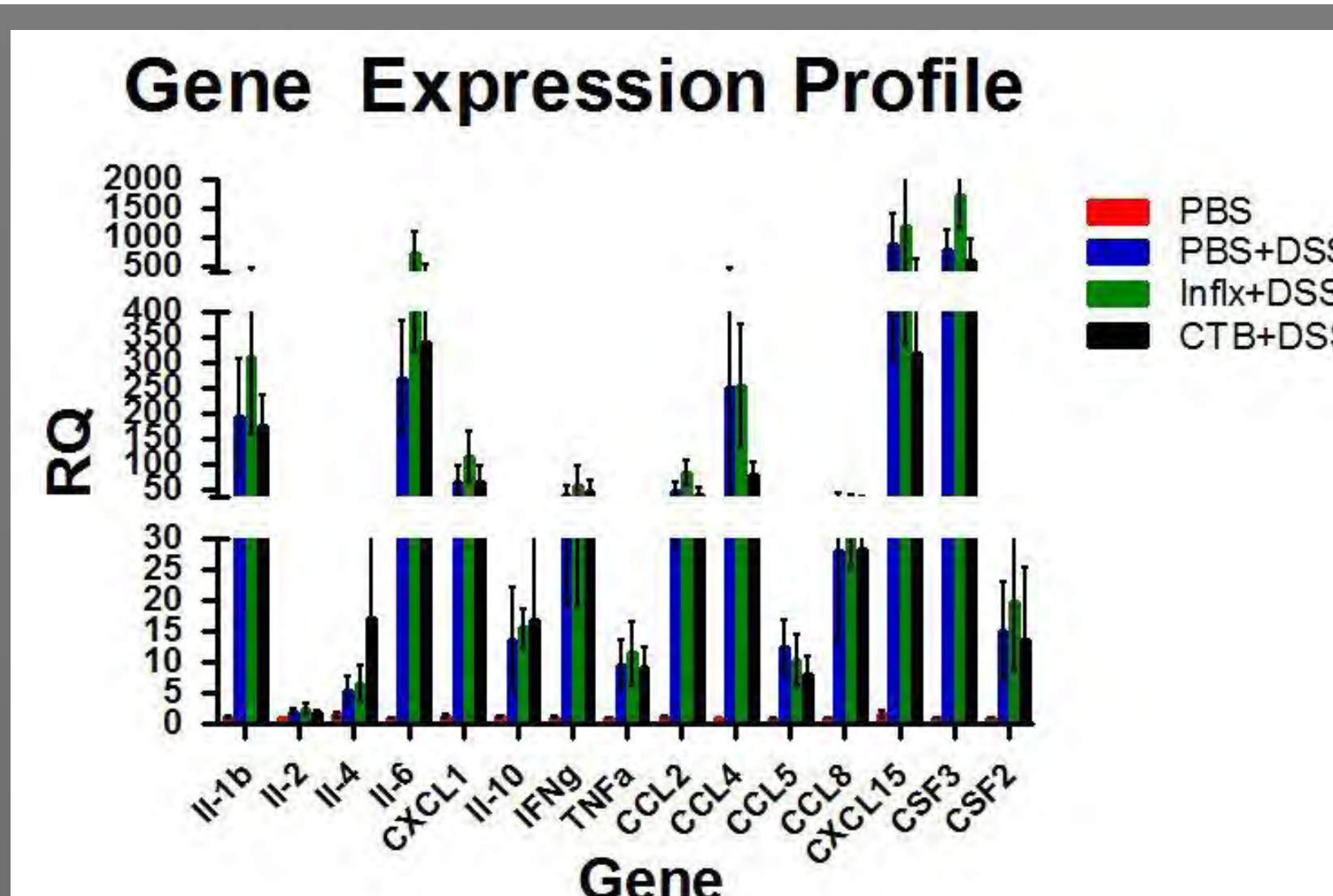


Figure 6. Gene expression profile. Expression levels of the 15 genes listed above were analyzed by quantitative reverse-transcription PCR. Housekeeping genes : 18S rRNA, GAPDH, and ACTB. Five samples from each of the 4 groups were analyzed.

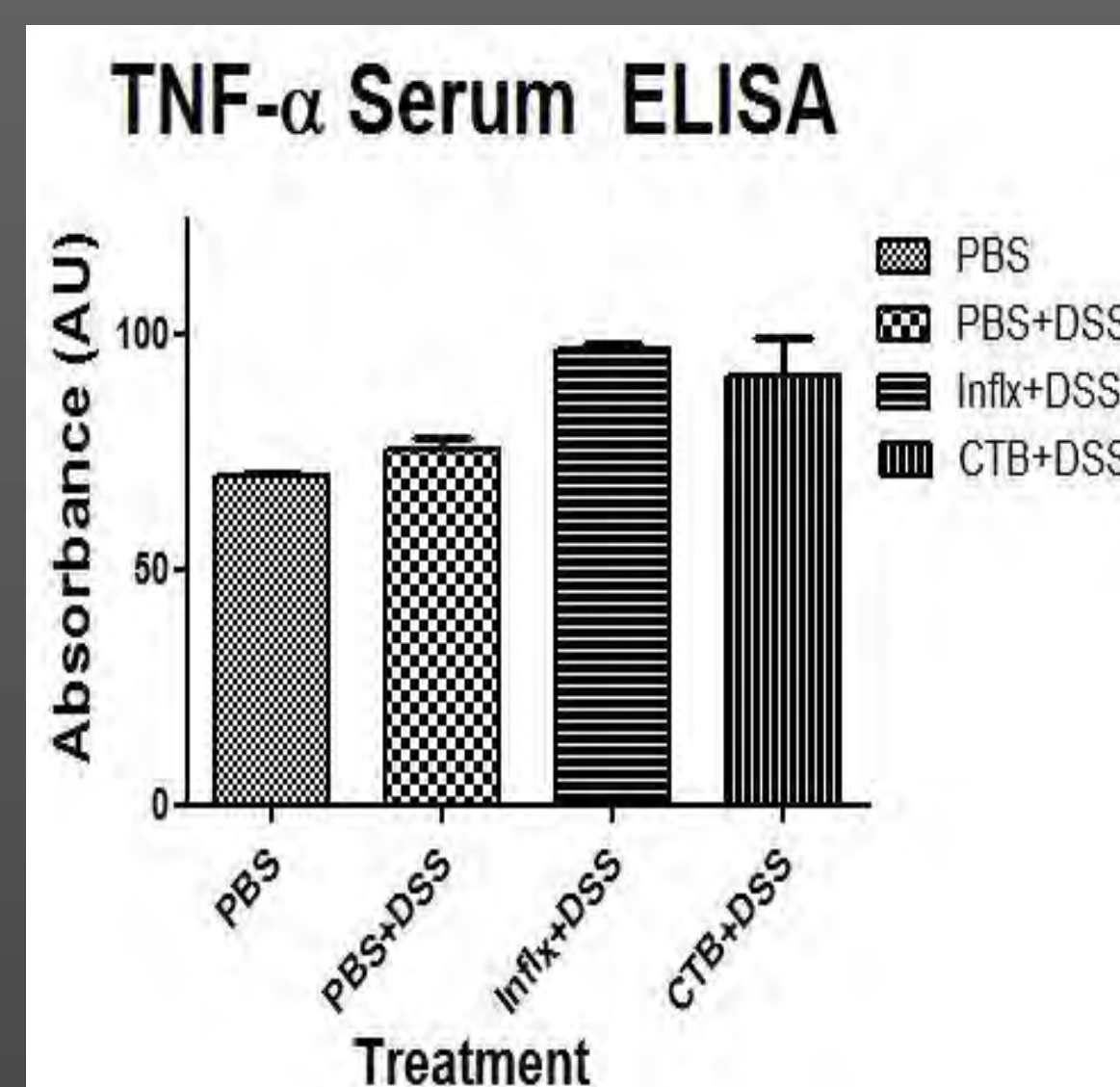


Figure 7. Preliminary TNF-α Serum ELISA. A one-way ANOVA shows no statistically significant difference between any of the treatment groups for TNF-α levels in serum. Signals were weak, if not absent for all samples.

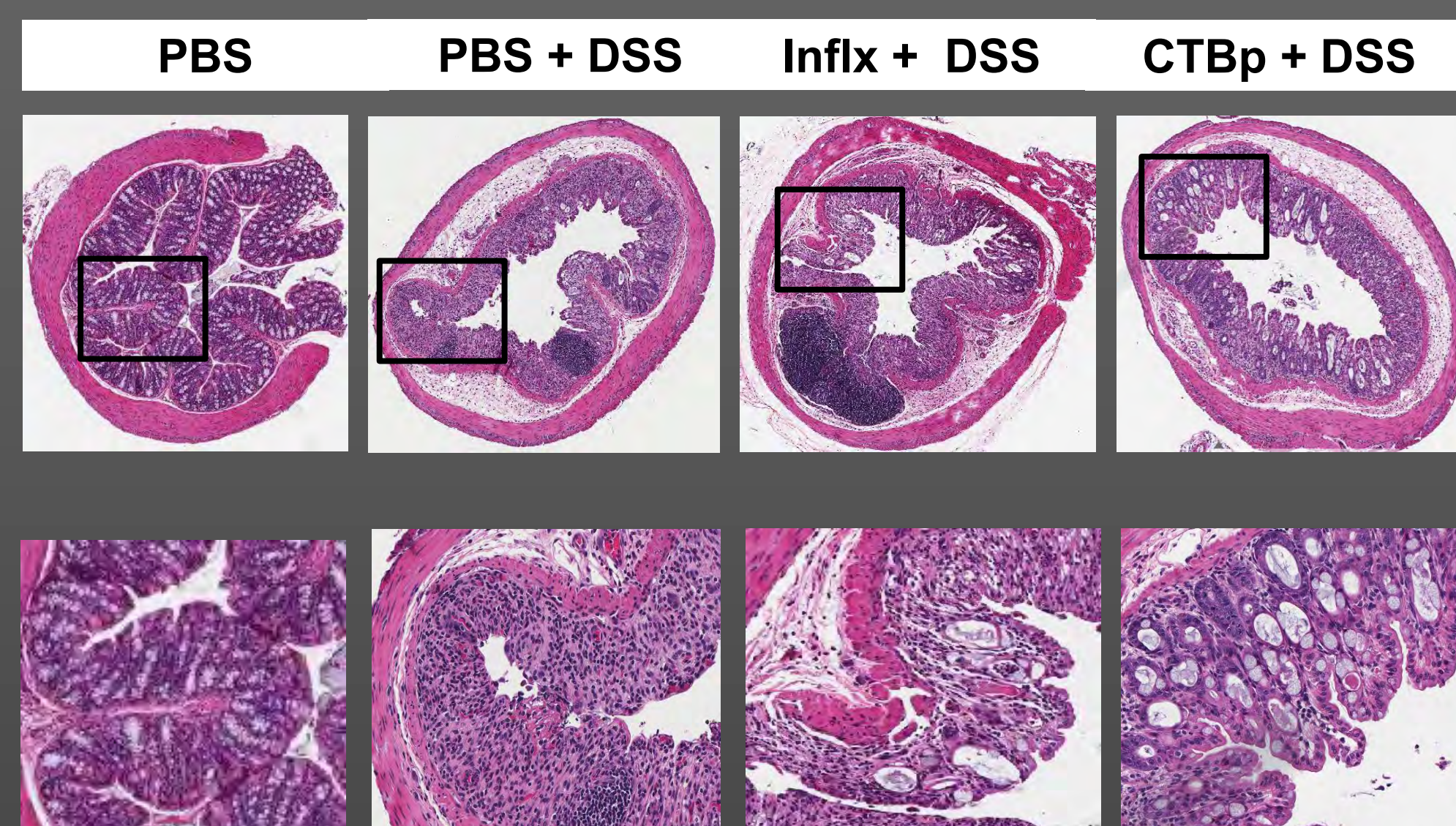


Figure 8. Maximum Inflammation H&E staining. Representative composite photomicrographs depicting PBS, PBS + DSS, Infliximab, and 3µg CTBp. 3% DSS exposure resulted in a loss of epithelial integrity, increased neutrophil infiltration and ulceration. In parts of the distal colon sections CTBp and Infliximab decreased inflammation injury, but in other parts of the sections neither treatment significantly blunted inflammation or ulceration.

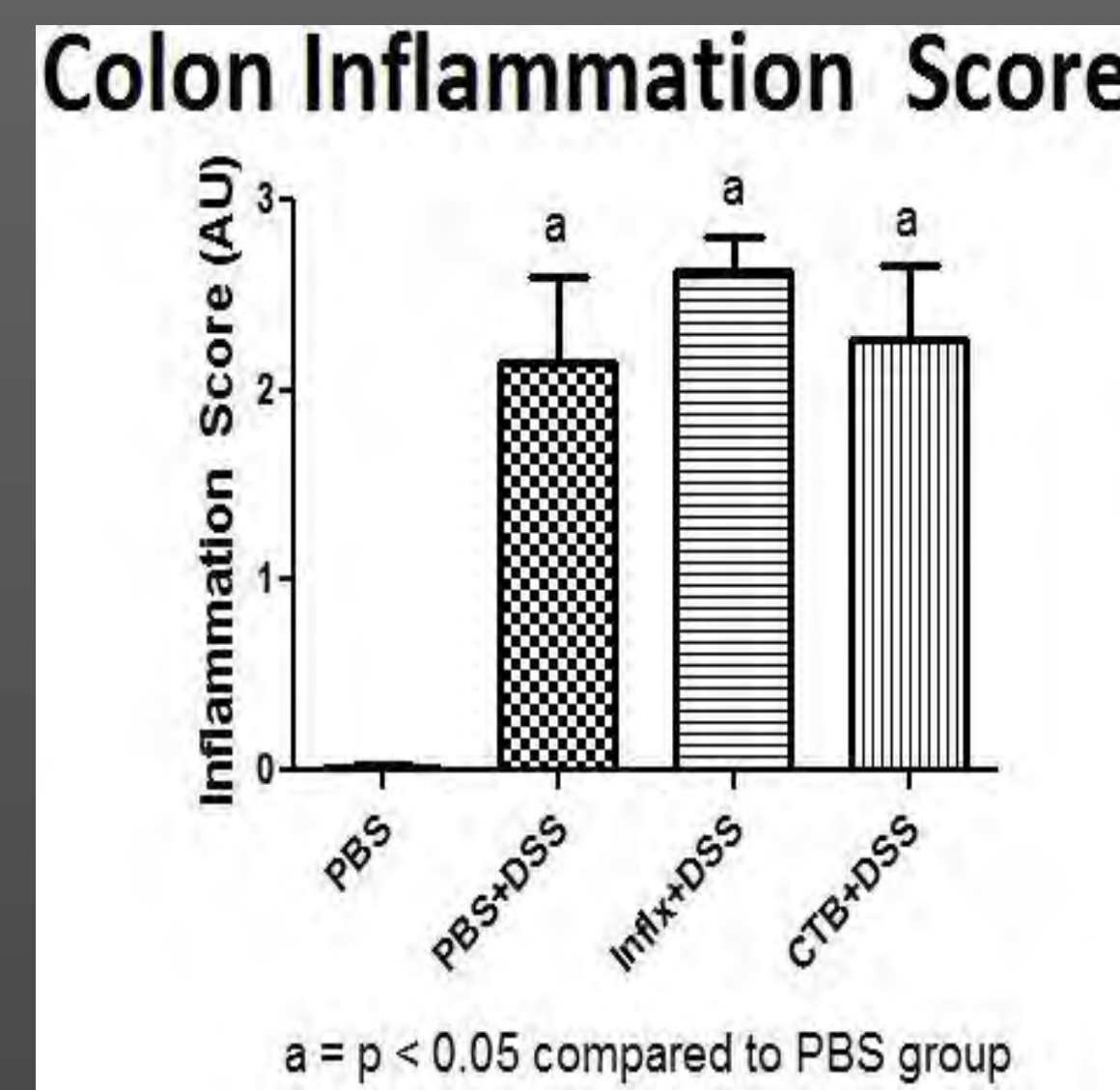


Figure 9. Maximum Inflammation Scoring. Mice were exposed to 3% DSS for 7 days. Inflammation scoring of H&E sections. One-way ANOVA with Bonferroi post-tests was performed: a = p < 0.05 compared to PBS.

Conclusions and Future Studies

Conclusions

- Treatment with 3µg CTBp significantly decreased the DAI when compared to Infliximab and PBS+DSS treatment.
- However, treatment with 3µg CTBp did not significantly blunt colon inflammation or decrease percent body weight loss when compared to PBS+DSS treatment.
- Treatment with 3µg CTB showed a trend of a decrease in many inflammatory genes and chemokines compared to PBS+DSS, while a single dose of 5mg/kg Infliximab did not.

Future Studies

- Additional studies are ongoing with different dose levels and timing to find an effective dosing regimen of CTBp.
- Comprehensive analyses of TNF-α and other cytokine levels in serum and tissue will be performed.

Acknowledgements

Research supported by a grant from University of Louisville Cancer Education Program NIH/NCI (R25-CA134283), the Helmsley Charitable Trust Program and DoD/USAMRMC/W81XWH-10-2-0082-CLIN2. CTBp was produced and validated by Krystal Hamorsky and Lauren Bennett at OCRP.

Materials and Methods

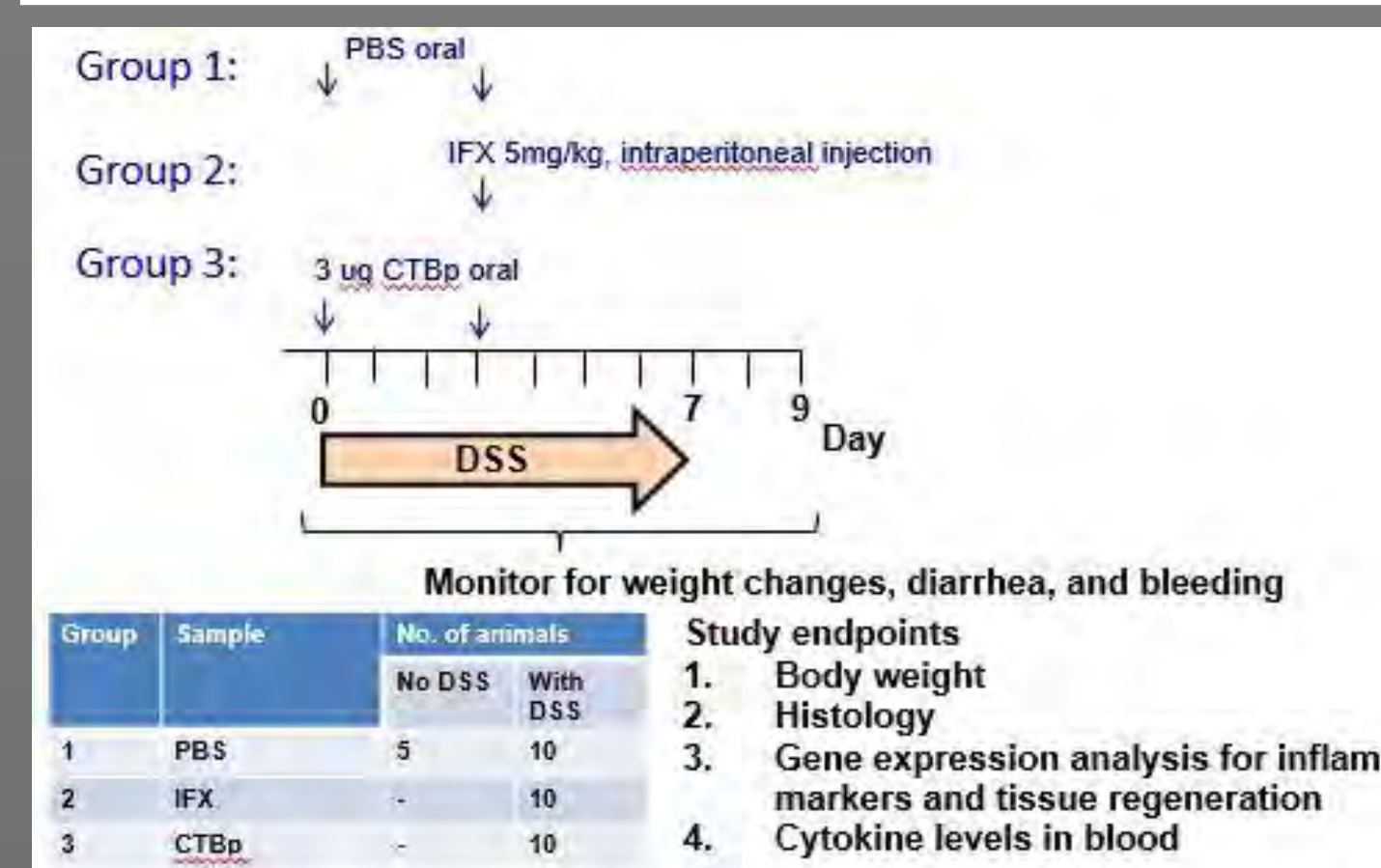


Figure 10. Experimental Design for Infliximab (Remicade®) and CTBp Comparison. Sodium bicarbonate was administered orally prior to PBS or CTBp (3µg) to neutralize stomach pH. PBS or CTBp were administered orally the day of the initiation of DSS exposure and the third day of DSS exposure. Infliximab (5mg/kg) was administered via an intraperitoneal injection on the third day of DSS exposure. 3% DSS was administered for 7 days and followed by a 2 day recovery period. Mice were sacrificed 9 days after the initiation of the experiment.

Animals and treatments. Eight week old female C57BL/6J mice were ordered from Jackson Laboratory (Bar Harbor, ME). Animals were given oral (gavage) doses of CTBp (3µg) or PBS two times during DSS exposure, or an intraperitoneal injection of Infliximab (5 mg/kg) on the third day of DSS exposure (see Figure 2).

Percent Body Weight Change. Initial body weights were collected immediately prior to the initiation of DSS exposure. Body weights were collected in the same time frame daily and the percent change from the baseline (initial body weight prior to exposure to DSS) were calculated.

Disease Activity Index (DAI) Scoring. The DAI score is based on a combination of stool consistency, percent body weight change on the day of the sacrifice (day 9) and blood in the stool. Blood in the stool was analyzed with a ColoScreen 1000™ occult blood test from Helena Laboratories(Beaumont, TX). Scoring guidelines are as follows:

Body Weight	Stool Consistency	Blood in Stool
0= no weight loss	0= normal	0= no bleeding
1= 1%-5% weight loss	1= loose stools	1= + occult blood test
2= 6%-10% weight loss	2= diarrhea	2= + occult blood test (max color change)
3= 11%-15% weight loss		3= blood visible in stool
4= >15% weight loss		4= gross anus bleeding with clotting

Gene Expression analysis. cDNA was synthesized from RNA isolated from the most distal section of five mice from each of the four groups using Invitrogen™'s SuperScript® VILO™ cDNA Synthesis Kit (Carlsbad, CA). RNA was added at concentration of 600µg. An Applied Biosystems™'s Custom TaqMan® Gene Expression Assay was used in qPCR to quantify gene expression (Carlsbad, CA). cDNA was diluted 2.1 fold and qPCR was performed in a 7500 Fast system Real-Time PCR System. Thermal-cycling profile: UNG Incubation for 2 minutes, Polymerase activation for 20 seconds followed by 40 PCR cycles (denature for 3 seconds and anneal for 30 seconds).

Cytokine Levels in Blood. TNF-α protein levels in mice serum for each mouse were measured using eBioscience®'s Mouse TNF alpha ELISA Read-SET-Go! Kit® (San Diego, CA).

Hematoxylin and Eosin Staining. Tissue sections of the distal colon were collected on the day of the sacrifice and placed in 10% formalin for 18 hours. The tissue was transferred into 70% ethanol until the time of paraffin embedding. The paraffin embedding, cutting, and H&E staining were all performed by a trained professional. The tissue sections were scanned on an Aperio Scan Scope C5 for analysis.

Colon Inflammation Scoring. Distal colon tissue sections with H&E staining were scored based on the guidelines provided by Cooper *et al.* (1993). One tissue section was divided into ten parts with each part receiving a score (0/Control to 4) and the total tissue score being a mean of those scores.

Statistics. Summary data are means ± SEM. One-way or two-way ANOVA with Bonferroi's post-hoc test were used for the determination of statistical significance among treatment groups, as appropriate, using GraphPad Prism 5 software.

References

- **Figure 1.** <http://www.ncbi.nlm.nih.gov/Web/News/Summer00/images/cholera2.gif>
- Bauldauf, K.J., Kouokam, J.C., Bodduluri, H., & Matoba, N. A plant-produced Cholera Toxin B Subunit Prevents Acute Colitis in a Mouse Model. Poster.
- Boirivant, M., Fuss, J.J., Ferroni, L., Pascala, MD., & Strober, W. Oral administration of Recombinant Cholera Toxin Subunit B Inhibits IL-12-Mediated Murine Experimental (Trinitrobenzene Sulfonic Acid) Colitis. *J Immunol.* 166, 3522-3532 (2001).
- Hamorsky, K.T., Kouokam, J.C., Bennett, L.J., Baldauf, K.J., Kajjura, H., Fujiyama, K., Matoba, N. Rapid and Scalable Plant-based Production of a Cholera Toxin B Subunit Variant to Aid in Mass Vaccination against Cholera Outbreaks. *PLoS Negl Trop Dis.* 7(3), e2046 (2013).
- Smits, H.H., Gloudemans, A.K., van Nimwegen, M. Willart, M.A., Soullie, T., Muskens, F., et al. Cholera Toxin B Subunit suppresses allergic inflammation through induction of secretory IgA. *Mucosal Immunol.* 4, 331-339 (2009).
- Sun, J.B., Czerkinsky, C., Holmgren, J. Mucosally induced immunological tolerance, regulatory T cells and the adjuvant effects of Cholera Toxin B Subunit. *Scand J Immunol.* 71(1), 1-11 (2010).

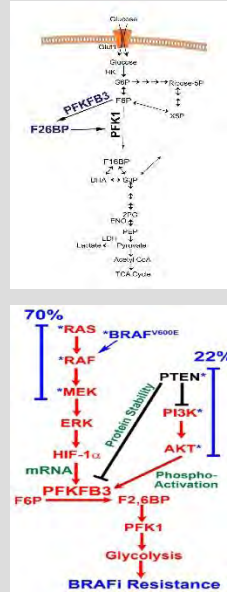
Inhibition of PFKFB3 and BRAF^{V600E} may be an effective treatment for metastatic melanoma

Conor O'Neill, Julie O'Neal, and Jason Chesney
Department of Medicine, University of Louisville

Abstract

In human cancers, rates of glycolysis have been shown to increase up to 200 times in order to achieve high rates of proliferation and survival. One key regulator, 6-phosphofructo-2-kinase (PFKFB3) phosphorylates fructose-6-phosphate (F6P) to produce fructose 2,6-bisphosphate (F26BP), a potent activator of 6-phosphofructo-1-kinase (PFK1), that regulates an irreversible step of glycolysis. Oncogenes and various tumor suppressor genes regulate PFKFB3 (i.e. PTEN, RAF/BRAF, Hif1 α). A promising drug, PFK-158 that inhibits PFKFB3 is currently in Phase I clinical trials. About half of metastatic melanomas express a mutant form of B-RAF (*BRAF^{V600E}*) and those patients are treated with Vemurafenib (VEM) or Dabrafenib; both are specific inhibitors of mutant B-RAF kinase activity. However, up to 50% of patients treated with VEM respond, but then relapse while the other 50% are intrinsically resistant to VEM. Since *BRAF^{V600E}* promotes glucose metabolism, survival and growth, and regulates Hif1 α , we hypothesized that *BRAF^{V600E}* regulates glycolysis through PFKFB3. Knockdown of *BRAF^{V600E}* with specific siRNA's mimicked the glycolytic effect of VEM including down-regulating PFKFB3. To our surprise, overexpressing *BRAF^{V600E}* had little effect on PFKFB3 in cells expressing WT BRAF. Lastly, combination treatment with VEM and PFK-158 in VEM resistant cells that express *BRAF^{V600E}*, resulted in synergistic cell death. Our data suggest VEM + PFK-158 may be a promising treatment option for metastatic melanomas resistant to Vemurafenib.

Background

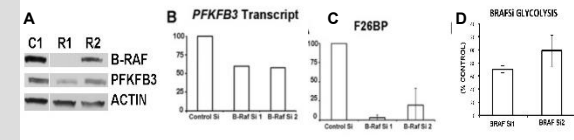


- PFKFB3 phosphorylates F6P → F26BP an allosteric activator of PFK1
- PFKFB3 is highly expressed in human cancer and tumorigenic growth
- BRAF^{V600E} regulates Hif1 α , which regulates PFKFB3
- Hypothesis: BRAF^{V600E} regulates PFKFB3 via Hif1 α

Results

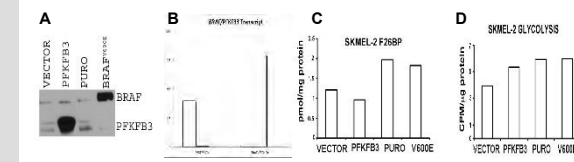
Approach: A375 melanoma cells are homozygous for BRAF^{V600E} making them a good model system for understanding effects BRAF^{V600E} knockdown.

Figure 1. Knockdown of BRAF^{V600E} in A375 cells mimics inhibition of BRAF^{V600E} by Vemurafenib. A375 cells were plated and treated with BRAF siRNAs or Control Si RNA molecules for 48 hours. Cells were harvested and assayed for **A.** BRAF and PFKFB3 Protein, **B.** PFKFB3 transcripts **C.** F26BP levels **D.** Glycolysis.



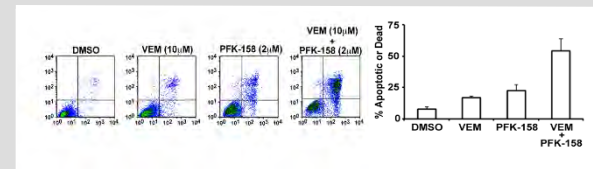
Approach: SK-MEL-2 melanoma cells express wild-type BRAF so were chosen for BRAF^{V600E} overexpression studies to assess its effect on PFKFB3 expression and PFKFB3 functions including F2,6BP production and glycolysis

Figure 2. Overexpression of BRAF^{V600E} in SK-Mel-2 cells had little effect on PFKFB3 expression and glycolysis. Cells were harvested and assayed for **A.** BRAF and PFKFB3 Protein, **B.** PFKFB3 and BRAF^{V600E} transcripts **C.** F26BP levels **D.** Glycolysis.



Approach: A2058 melanoma cells are homozygous for BRAF^{V600E} but resistant to Vemurafenib so were used for testing whether PFK158 (PFKFB3 inhibitor) and Vemurafenib would result in synergistic cell death.

Figure 3. Synergistic death in A2058 (VEM resistant) cells with PFKFB3 inhibitor (PFK158) and Vemurafenib. 10,000 cells were plated and treated with DMSO, VEM, PFK158, or both. 72 hours later, cells were harvested, stained with Annexin V, and Propidium iodide and apoptosis and death were quantitated using FlowCytometry.



Conclusions

- BRAF^{V600E} knockdown in A375 cells reduced PFKFB3 and F2,6BP levels suggesting BRAF^{V600E} regulates PFKFB3
- Overexpression of BRAF^{V600E} did not lead to an increase in PFKFB3 expression, F2,6BP levels, or an increase in glycolysis.
 - We hypothesize that endogenous wild-type BRAF^{V600E} is having a dominant negative effect
 - Experiments to knockdown endogenous and overexpress BRAF^{V600E} are underway
- Synergistic cell death was observed when the VEM resistant cell line (A2058) was treated with VEM and PFK158.
 - We hypothesize this is due to complete inhibition of glycolysis and will test this in the future.

Acknowledgements

Research supported by a grant from R25-CA-134283 from the National Cancer Institute, & the University of Louisville Cancer Education Program.

Circadian Disruption: distress and sleep quality in breast cancer patients



Thomas Packer, BA¹, Lauren A. Zimmaro, BA¹, Elizabeth Cash, PhD^{1,2}, and Sandra E. Sephton, PhD^{1,2}

¹ Department of Psychological and Brain Sciences, University of Louisville, Louisville, KY.

²J.G. Brown Cancer Center, University of Louisville, Louisville, KY

ABSTRACT

Breast cancer is the most common form of cancer and second leading cause of cancer deaths among women of all races. The distress accompanying a cancer diagnosis and its affect on circadian rhythmicity has not been fully explored. We tested for the predictability of circadian activity measures based on the psychosocial factor of distress. Our assumptions were based on a model of tumor progression (Eismann, et al., 2010). Forty-eight breast cancer patients completed an Impact of Event Scale self-report to measure their subjective response to their cancer diagnosis. A multiple regression analysis controlling for age was used to predict each measure. Actigraphy is the recording of body movement that provides a noninvasive measure of rest-activity rhythms and sleep patterns. Participants wore a wristwatch-like device (Motionlogger) continuously for four days. Whenever the device moves, a piezoelectric beam generates voltage signals that are recorded in 60-second segments, creating a curve scored as “wake” or “sleep”. The circadian rhythm in activity was estimated using the autocorrelation coefficient calculated based on 24-hour time lags. We hypothesized that total distress would be associated with circadian rhythmicity, sleep efficiency, amount of time spent awake after sleep onset, amount of time spent sleeping, and the number of nightly awakenings. After statistical analysis, total distress scores alone were incapable of predicting circadian disruption in any of the measures tested. Total distress as reported from the IES did not show significant proportion of variance in circadian activity measures.

BACKGROUND

Breast cancer is the most common form of cancer and second leading cause of cancer deaths among women of all races. 1 in 8 American women will develop invasive breast cancer over the course of her lifetime. While about 5-10% of breast cancers can be explained by mutations in the BRCA1 and BRCA2 genes, mutations in circadian regulatory genes as are increasingly being studied as alternative causes for tumor development and metastasis.

Circadian regulatory genes such as PER3 and NPAS2 are responsible for regulating the endogenous 24 hour sleep wake cycle (circadian rhythm) that maintains sleep, wakefulness, hormone biosynthesis, metabolism, and immune response. Abnormal circadian rhythms have been associated with higher risk of cancer development with faster tumor growth and shorter survival. Survival at 2 years was greatest for those with a normalized activity rhythm.

Disrupted circadian function has been correlated with poor sleep, fatigue, and depression. Patients with marked rest/activity rhythms also have better quality of life and report significantly less fatigue. Studies have shown that circadian activity correlates with several health related quality of life scales. A cancer diagnosis can be stressful for an individual. This is why cancer diagnoses are commonly accompanied by psychological distress caused by anxiety and depression some time after the initial diagnosis. Psychological distress is a known deregulator of endocrine and immune function, while possibly even affecting cortisol and circadian rhythms. Activity/Disruption will be associated with distress as measured by the self report Impact Event Scale (IES)

ABSTRACT

•Subject participation criteria: patients must:

- Be over age 18 and under age 85
- Have received a diagnosis of non-small cell lung cancer within the previous five years
- Have no concurrent medical diagnosis likely to influence short-term (6-month) survival.

•All participants were provided with a \$100 gift card at completion of data collection.

•Measures:

- **Impact of Event Scale (IES):** 48 Participants were provided with an IRB approved IES self report packet that measures self reported distress.
 - Questionnaire uses a specific traumatic event as a reference within the time frame of the past seven days.
 - The subscales measures different dimensions of stress response but are scored together to form an overall total distress score.
 - IES score data was organized into 4 groups lifted from literature and based on severity of self report distress scores
- **Actigraphy**→Actigraphy is the recording of body movement that provides a noninvasive measure of rest-activity rhythms and sleep patterns.
 - Circadian activity measures were circadian rhythmicity, sleep efficiency, amount of time spent awake after sleep onset, amount of time spent sleeping, and the number of nightly awakenings
 - In this study, body movements were recorded by a device called the Motionlogger.
 - Actigraphs were worn on participants’ wrists continuously for 4 days.
 - A piezoelectric beam generates voltage each time the device moves.
 - This motion are recorded in 60-second segments, with voltage signals from each minute creating a curve, allowing for calculation of area under the curve (AUC).
 - Segments are scored as “wake” or “sleep” using calculations based on the University of California – San Diego (UCSD) Sleep Scoring Algorithm.
 - The circadian rhythm in activity was estimated using the autocorrelation coefficient calculated based on 24-hour time lags, with strong circadian rhythms expected to be associated with increased autocorrelation coefficients. Action 4 software allowed for comprehensive and reliable measurement of circadian rhythm coordination and total sleep time.

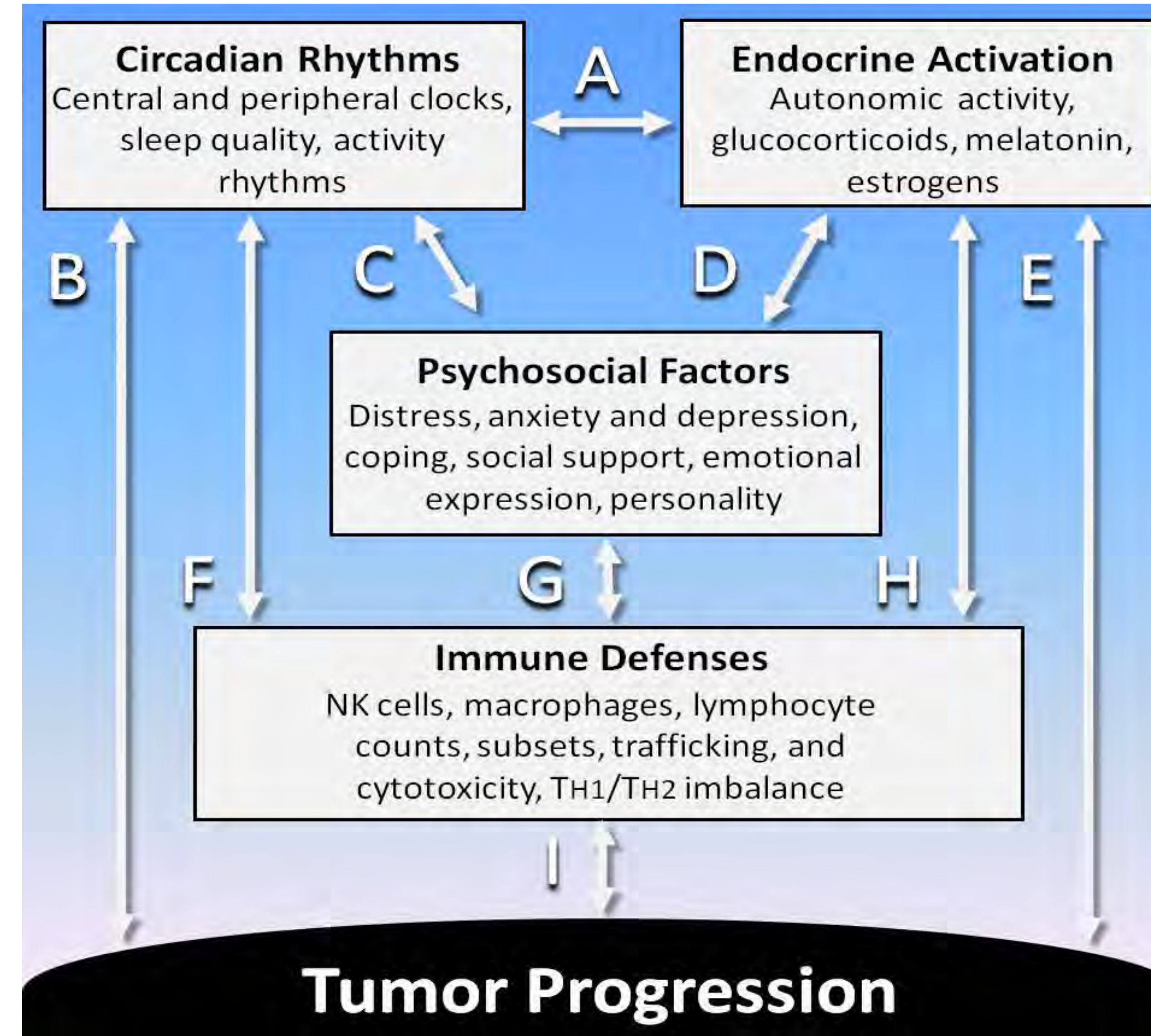


Figure 1. A model of circadian effects in cancer-relevant psychoneuroendocrine and immune pathways (Eismann, et al., 2010).

Demographics		
Ethnicity	Frequency	Percent
Asian	1	2.1
Black	16	33.3
Native American	2	4.2
White/Caucasian	29	60.4
Total	48	100
Gender	Frequency	Percent
Female	48	100
Age (Mean)	Minimum	Maximum
51.69	21	79

Figure 2. Population demographics

Descriptive Statistics				
Measure	N	Mean	Std. Deviation	Variance
IES total distress	48	30.0833	14.95644	223.695
24 hour autocorrelation coefficient	48	0.28207864	0.161419881	0.026
Overall sleep efficiency	48	0.8863	0.09698	0.009
Nightly awakenings # (mean)	48	11.9861	5.3039	28.131
Sleep time (mean)	48	385.4809	80.1358	6421.747
Nightly awake time (mean)	48	46.9441	36.29164	1317.083
Age at diagnosis	48	51.69	13.628	185.709

Figure 3. Descriptive Statistics of variables

RESULTS

ANOVA							Coefficients		
Predictor	Model	df	F	Sig.	R	R ²	Beta	t	Sig.
Auto Correlation coefficient	Regression	2	0.168	0.846	0.086	0.007396	0.063	0.422	0.675
	Residual	45							
	Total	47							
Overall Sleep Efficiency	Regression	2	0.274	0.762	0.11	0.012	-0.11	-0.74	0.463
Nightly Awakenings # (mean)	Regression	2	1.041	.361c	0.21	0.044	0.19	1.301	0.2
Sleep Time (mean)	Regression	2	0.408	.667c	0.133	0.018	-0.089	-0.599	0.552
Nightly Awake Time (mean)	Regression	2	1.007	0.373	0.207	0.043	.128b	0.876	0.386

Figure 4. Multiple Regression Statistical Analysis

RESULTS

- Total Distress did not significantly predict autocorrelation coefficient values, $\beta=0.063, t(0.422)=0.675$ and did not show significant variance $R^2 = 0.17, F(2,45)=0.388 p >0.05$
- Total Distress did not significantly predict overall sleep efficiency $\beta=-0.11, t(-0.74)=0.463$ and did not show significant variance $R^2 = 0.012, F(2,45)=0.274 p >0.05$
- Total Distress did not significantly predict amount of time spent awake after sleep onset $\beta=0.063, t(0.422)=0.675$ and did not show significant variance $R^2 = 0.043, F(2,45)=1.007 p >0.05$
- Total Distress did not significantly predict amount of time spent sleeping $\beta=-0.089, t(-0.599)=0.552$ and did not show significant variance $R^2=0.018, F(2,45)=0.408 p >0.05$
- Total Distress did not significantly predict the number of nightly awakenings $\beta=0.19, t(1.301)=0.2$ and did not show significant variance $R^2=0.044, F(2,45)=1.041 p >0.05$
- Grouped IES data was grouped and analyzed via MANOVA analysis but showed no significance within or between groups.

DISCUSSION

- Total distress score alone is not enough to predict circadian disruption.
 - Only by grouping the self report scores by their distress severity was it possible to see the slightest correlation between total distress and circadian rhythmicity.
 - While not statistically significant, it would be interesting to design an experiment around the parameters of stress severity (ordinal) and circadian disruption.
- All participants were provided with a \$100 gift card at completion of data collection.
- 24 hour autocorrelation (Daily circadian rhythmicity) should contribute to a persons ability to fall asleep naturally, but significant data was not obtained to support this notion.
 - More data with consistent normality is needed to explore this hypothesis further.
- There are some possible explanations for this non-significant data.
 - Extreme outliers made data analysis difficult because many of the measures did not assume normality.
 - Since these patients have only recently been diagnosed with cancer, it is possible their health had not deteriorated to a point which compromised their circadian rhythmicity
 - It’s possible there was error in collecting the self report data because of the mental health of the subject. This is an attractive explanation because all of the subjects were newly diagnosed cancer patients. The sudden mental distress may raise eyebrows on the accuracy of self report data if participants weren’t truly invested in data collection. In such situations, it would be beneficial to have many different measures of self report data.

Future Projects:

- This experiment is being repeated with an expanded IES and more psychosocial variables such as anxiety, depression, coping, and social support.
- Measures such as the Perceived Stress Scale (PSS) and the Symptom Distress Scale (SDS) can offer a more reliable and comprehensive self report into patient distress.
- Measures such as the Beck Anxiety Inventory (BAI), Beck Depression Inventory (BDI), Pittsburg Sleep Quality Inventory (PSQI) offer a chance to find more comprehensive relationships between variables such as anxiety, depression, and circadian disruption.
- There is interest in testing patients for mutations in circadian regulation genes PER3 and NPAS2

References

- ◆ CDC - Cancer Among Women. (2014/07/29/14:23:02). from <http://www.cdc.gov/cancer/dpce/data/women.htm>
- ◆ Savvidis, C., & Koutsilieris, M. (2012). Circadian Rhythm Disruption in Cancer Biology. *Molecular Medicine*, 18(1), 1249-1260. doi: 10.2119/molmed.2012.00077
- ◆ Dedert, E., Lush, E., Chaggar, A., Dhabbar, F. S., Segerstrom, S. C., Spiegel, D., . . . Sephton, S. E. (2012). Stress, coping, and circadian disruption among women awaiting breast cancer surgery. *Ann Behav Med*, 44(1), 10-20. doi: 10.1007/s12160-012-9352-y
- ◆ Eismann, E. A., Lush, E., & Sephton, S. E. (2010). Circadian effects in cancer-relevant psychoneuroendocrine and immune pathways. *Psychoneuroendocrinology*, 35(7), 963-976. doi: 10.1016/j.psyneuen.2009.12.011
- ◆ Filipski, E., King, V. M., Li, X., Granda, T. G., Mormont, M.-C., Liu, X., . . . Lévi, F. (2002). Host circadian clock as a control point in tumor progression. *Journal of the National Cancer Institute*, 94(9), 690-697.



Acknowledgments

Authors would like to thank National Cancer Institute grant R25-CA134283.

Henry Roberts BS¹, Jonathan Rice MD¹, Shesh Rai PhD², Jianmin Pan PhD², Robert Eichenberger MS¹, Susan Galandiuk MD¹

¹Hiram C. Polk Jr. MD Department of Surgery, University of Louisville School of Medicine, Price Institute of Surgical Research and the Section of Colorectal Surgery, Louisville, KY

²Department of Bioinformatics and Biostatistics, University of Louisville School of Public Health & Information Sciences, Louisville, KY

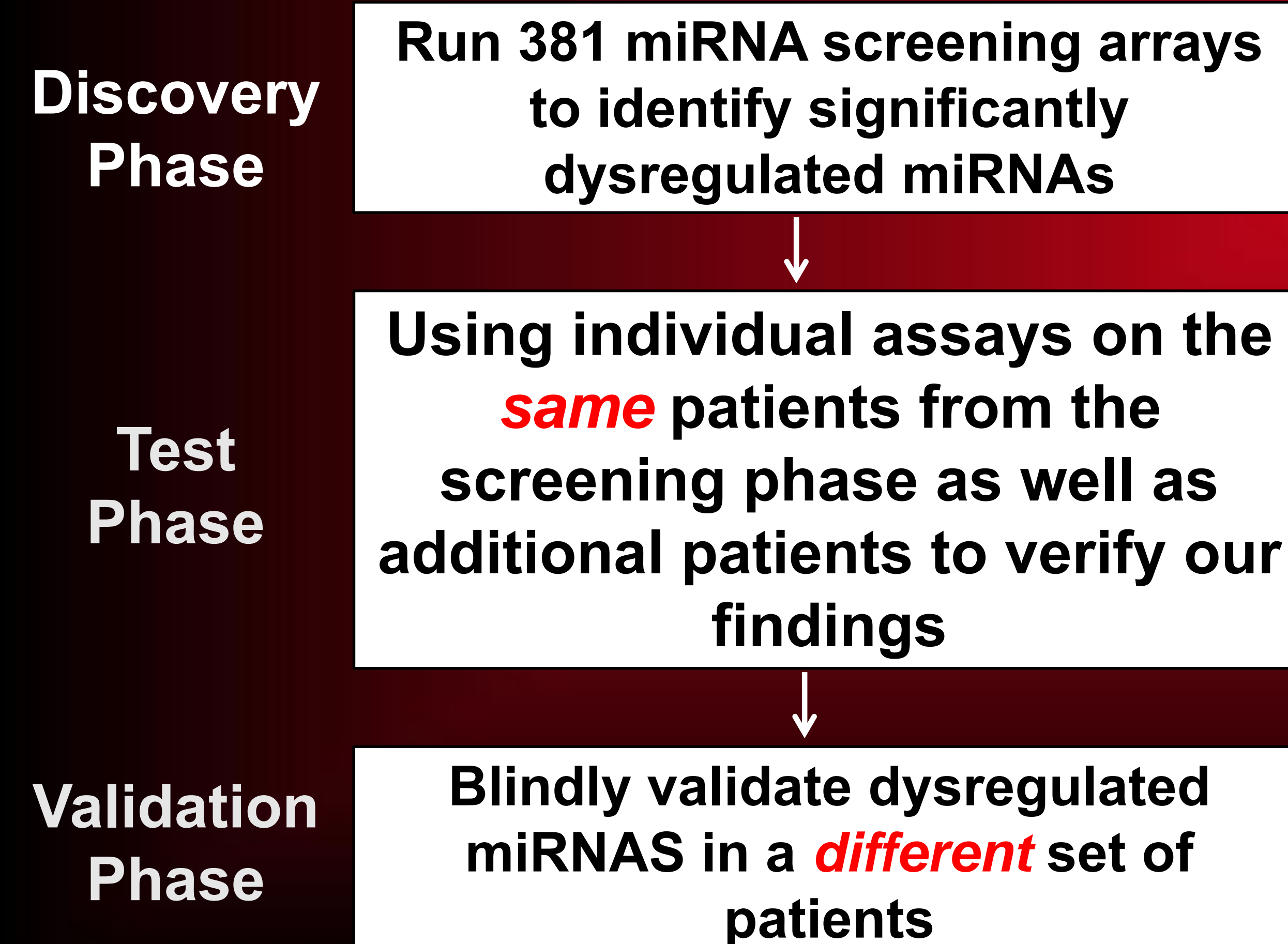
Introduction

- Colorectal cancer (CRC) is the third most common cancer worldwide
- Detection of colorectal adenomas (CRAd) is key to reduce the incidence and mortality of CRC
- Current methods of CRC screening (colonoscopy and fecal occult blood test) have many shortcomings thus there exists a need for a non-invasive biomarker with high sensitivity and specificity for the diagnosis of CRAd and CRC
- microRNAs (miRNAs) are short, non-coding RNA molecules approximately 22 nucleotides in length, that bind to messenger RNA and block translation of proteins
- miRNAs are thought to be involved in the development and progression of CRC, making them potential biomarkers of early disease
- Numerous miRNAs have been reported in the literature to be significantly dysregulated in the plasma of many different cancer types (e.g. miR-21)

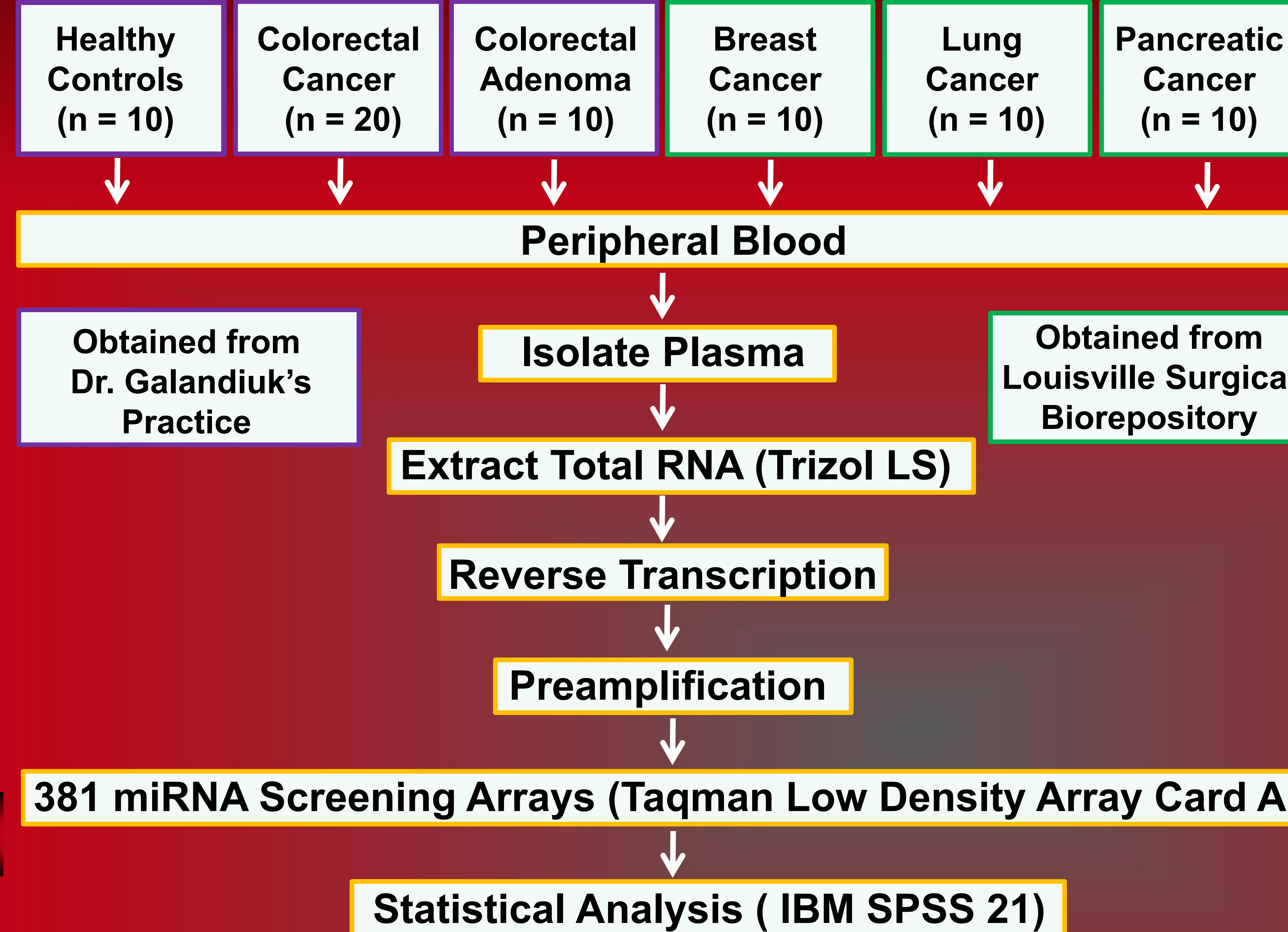
Hypothesis

We hypothesize that there exists a panel of miRNAs in plasma that is specific to colorectal neoplasia and would allow for a inexpensive, non-invasive and clinical useful detection method

Overall Study Design



Discovery Phase Study Design



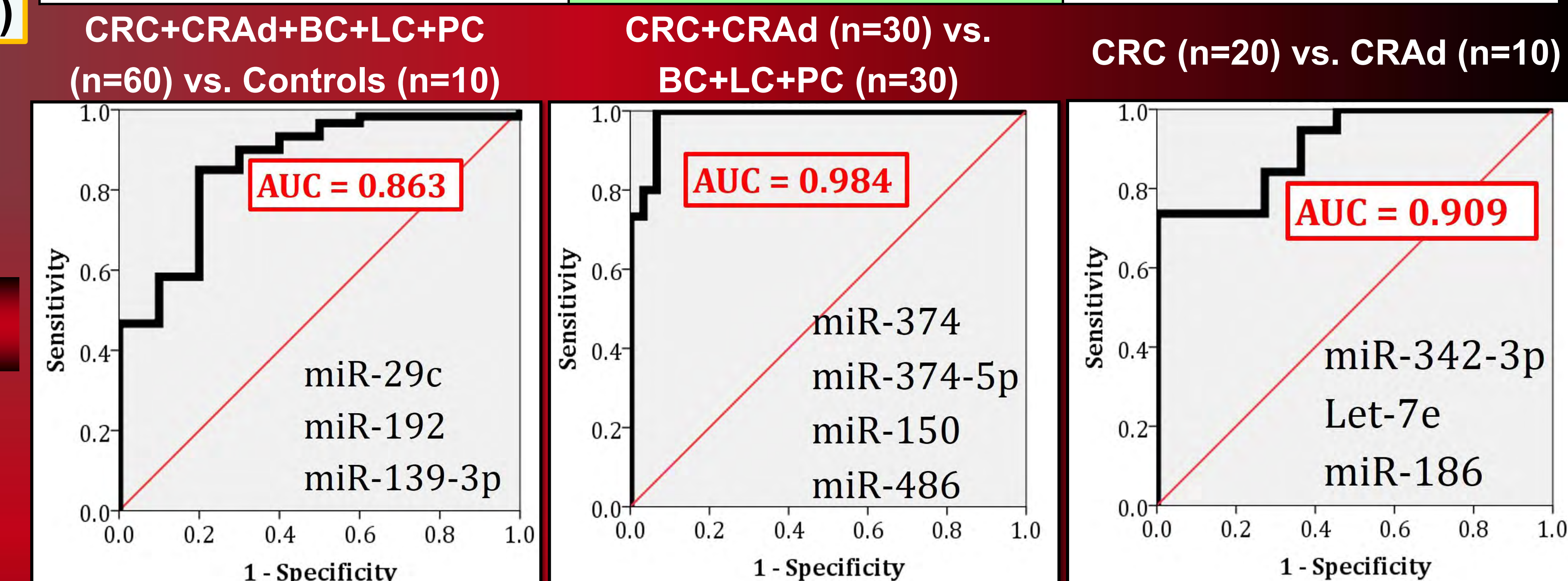
*All groups were age, race and gender matched to each other

Discovery Phase Statistical Analysis

- Each miRNA was normalized to the mean of U6 and miR-520d-5p (Δ CT)
- Three comparisons were performed
 - CRC+CRAd+BC+LC+PC (n=60) vs. Controls (n=10)
 - CRC+CRAd (n=30) vs. BC+LC+PC (n=30)
 - CRC (n=20) vs. CRAd (n=10)
- For each comparison
 - Only microRNAs with >90% expression were included in statistical analysis
 - Two-tailed students t-test with equal variance was performed to calculate p-value for Δ CT values
 - ROC curves were made using logistic regression model

Discovery Phase Results

Top 3 Significantly Dysregulated CRC+CRAd+BC+LC+PC (n=60) vs. Controls (n=10)		
microRNA	Fold Regulation	p-value
miR-29c	3.5	0.0002
miR-192	-11.3	0.0018
miR-139-3p	-1.1	0.0056
Top 4 Significantly Dysregulated CRC+CRAd (n=30) vs. BC+LC+PC (n=30)		
microRNA	Fold Regulation	p-value
miR-374	37.8	<0.001
miR-374-5p	329.8	<0.001
miR-150	2568.8	<0.001
miR-486	133.1	<0.001
Top 3 Significantly Dysregulated CRC (n=20) vs. CRAd (n=10)		
microRNA	Fold Regulation	p-value
miR-342-3p	5740.7	0.004
let-7e	12.1	0.004
miR-186	39878.8	0.007



Conclusions and Future Directions

The discovery phase for our plasma miRNA panel specific to colorectal neoplasia shows tremendous potential. These data will be verified and validated using individual miRNA assays in a larger test cohort (n=120) and double blinded validation cohort (n=150), respectively.

Acknowledgments

National Cancer Institute grant R25-CA134283, John W. and Caroline Price Family Trust as well as Donald and Irene Dizney

INTRODUCTION

Prostate Cancer as a Public Health Problem

Despite improvements in the early detection of prostate cancer (PCA) and treatment strategies, men with PCA stage 3 or higher have a 28% chance of survival 5 yrs after diagnosis.

Among PCA patients with stage 4 disease, there is a 90% chance that the tumor will spread to the bone. Bone specific metastasis is an aggressive disease that is non-responsive to conventional treatment.

New strategies are needed to improve the prevention/treatment of pre- and metastatic PCA.

Role of miRNAs as Prostate Cancer Biomarkers

Micro-RNAs (miRNA), short non-coding single stranded RNAs, may serve as effective tools to improve cancer diagnostic, prognostic, clinical management, and prevention strategies.

miRNAs function as oncogenes or tumor suppressors that are up- or down-regulated in various cancers, including prostate cancer, respectively.

Preliminary data generated by our lab suggest miRNA profiles (e.g., miR-106b and miR-186) were over expressed in the serum collected European American men diagnosed with metastatic and non-metastatic prostate cancer relative to controls. These same miRs were also over expressed in non-metastatic (E006AA) and/or metastatic prostate cancer cell lines (e.g., PC3).

miR-106b is one of three miRs (-25, -93, -106b) associated with the miR-25b cluster, which is overexpressed in many tumors

The over expression and under expression of oncomiRs and tumor suppressor miRs may counteracted by various chemopreventive agents, including Quercetin.

Quercetin as a chemopreventive agent

Quercetin is a flavonoid found in fruits (cranberry, black plums, strawberries, grapes, apples), vegetables (kale), leaves (e.g., radish, fennel), herbs (dill, cilantro), grains (e.g., buckwheat) and red wine.

This flavonoid has antioxidation, anti-inflammatory, anti-cancer properties

Quercetin inhibits cell invasion, migration, apoptosis, and/or cell proliferation in a metastatic PCA cell lines (e.g., PC-3).

Quercetin modulates the expression of genes involved in DNA repair, matrix degradation and tumor invasion, angiogenesis, apoptosis, cell cycle, cell matrix degradation, metabolism and glycolysis

Quercetin also acts as a bioavailability enhancer for many other substances by slowing their metabolic conversion to other substances.

Recent studies and clinical trials have confirmed claims that quercetin has activity against cancer tumors.

A few animal studies indicate that quercetin may alter the expression of oncogenic and tumor suppressing related miRNAs using *in vivo* studies.

However, it is not clear whether quercetin may be able to modulate the expression of miRNAs in a metastatic (i.e., PC-3) and primary PCA cell line derived from an African-American male (i.e., E006AA).

OBJECTIVES

To evaluate whether quercetin may modulate the expression of miR-186 and the miR-25b cluster (miR-106b, -25, -93)

Assess the impact of quercetin treatment (12.5-75µM) on cell proliferation and cell migration of E006AA (primary cancer cell line derived from an AA) and a metastatic PC3 prostate cancer cell lines

HYPOTHESIS

Quercetin will decrease prostate cancer cell proliferation and cell proliferation in the non- and metastatic prostate cancer cell lines.

Quercetin will decrease the expression of oncogenic related miRNAs (miR 106b, miR-186, miR-93, miR-25).

Alternatively, since miR-25 behaves as a tumor suppressor related miRNA, Quercetin treatment may down-regulate the expression of miR-25.

CLINICAL RELEVANCE

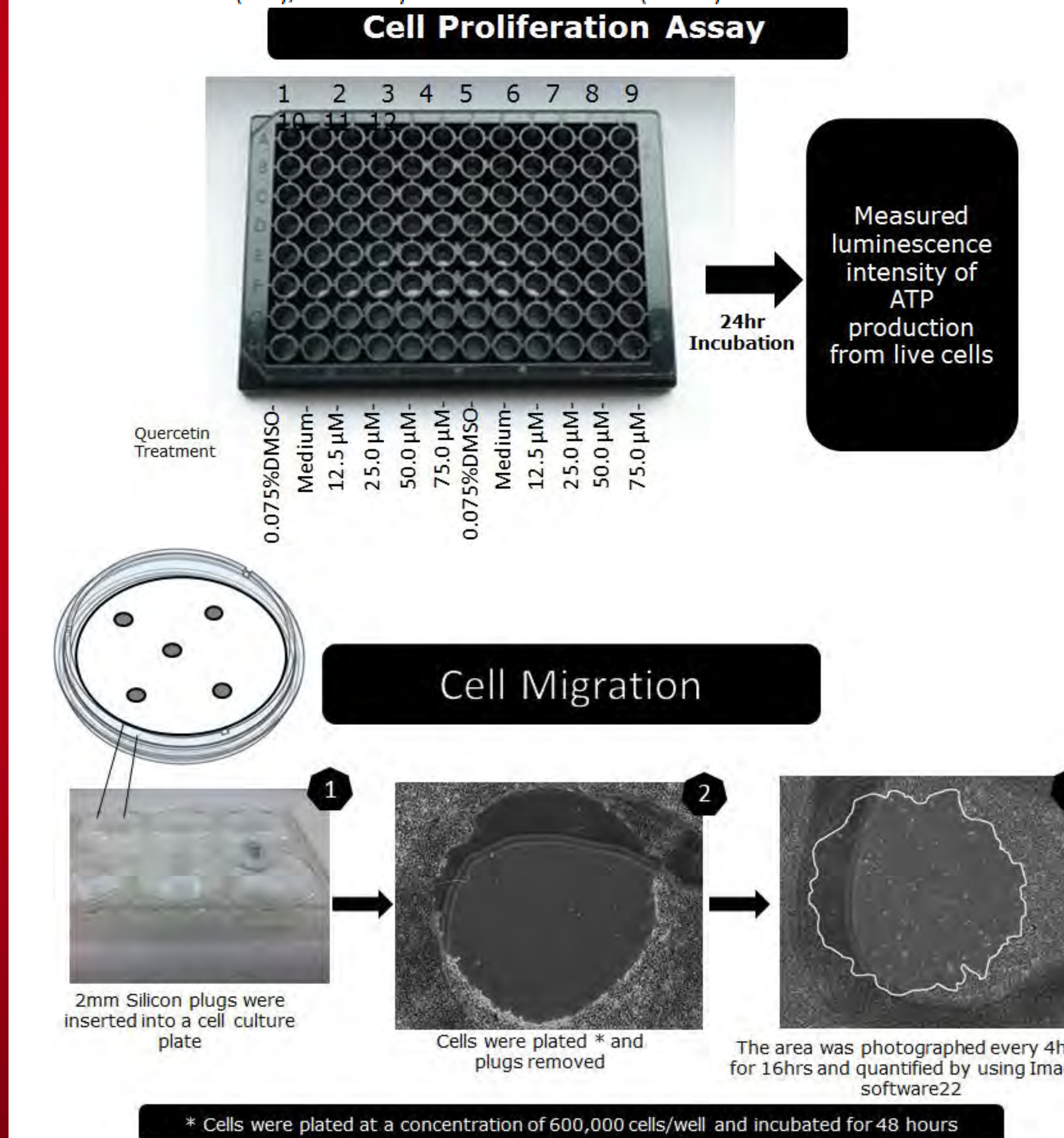
The findings of our study may serve as a foundation for future studies that seek to identify and validate new treatment strategies for individuals susceptible to pre- and metastatic PCA.

METHODS

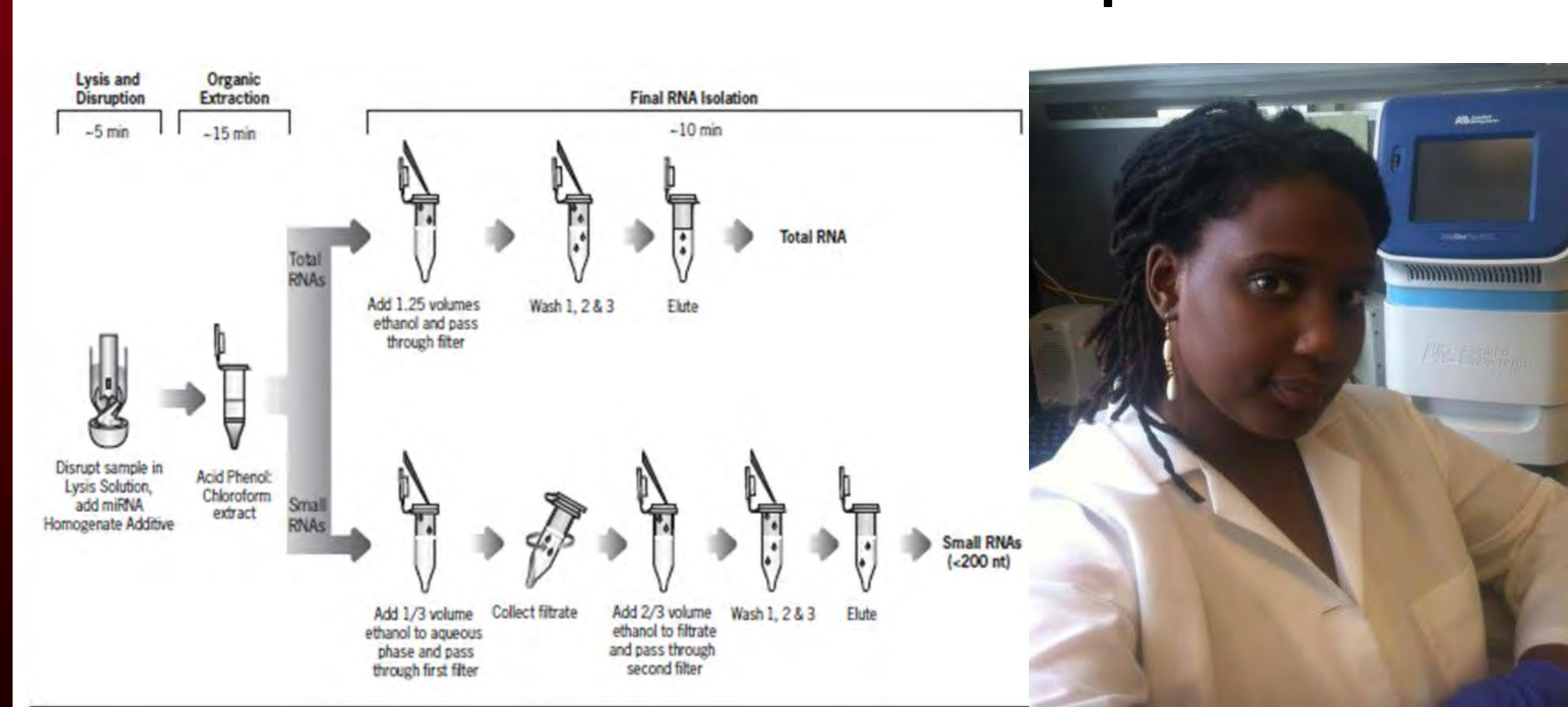
Table 1. Cell Culture

Cell Line	Disease/Site	Patient Age (yrs)/Ethnicity/Hormone dependence/Tumor Stage/ p53 Status	Tumorigenic (nude mice)	Cell Culture
E006AA	Prostate adenocarcinoma left middle lobe of prostate	50 African American AR+ Stage II p53 N/A	No	DMEM supplemented with 10% FBS* 1% L-glutamine and 1% antibiotic
PC3	Prostate adenocarcinoma bone metastasis	62 European-American AR- Stage IV p53 deficient	Yes	F12K* supplemented with 10% FBS* 1% L-glutamine and 1% antibiotic

*Fetal bovine serum (FBS), Keratinocyte serum free medium (K-SFM)



MirVana miRNA Isolation and qRT-PCR



RESULTS

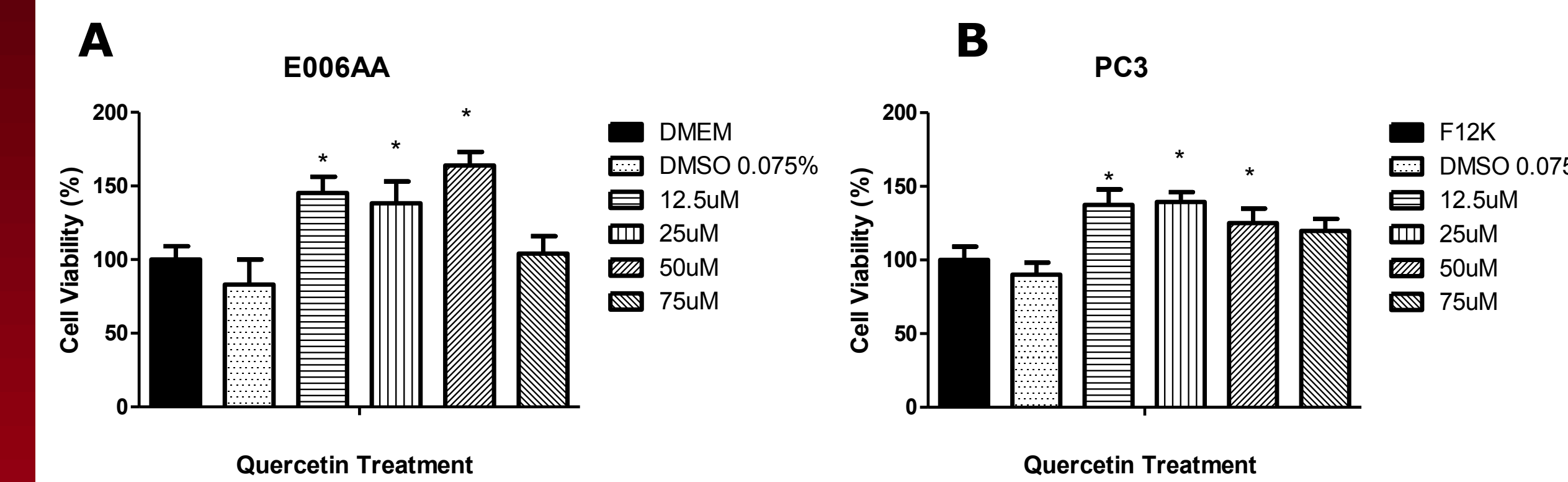


Figure 1. E006AA (A) and PC-3 (B) cells were treated with 12.5-75µM quercetin for 24 hours. Following quercetin treatments (12.5-50.0µM), cell viability was increased by 39-97% relative to the DMSO treated cells using E006AA (66-97%) and PC3 (39-54%) cell lines. However, at the highest quercetin dose (75µM) resulted in a non-significant 25% increase in cell viability compared to the DMSO control. There was a significant (-72%) decrease in cell viability for E006AA cell lines treated with 75µM of quercetin compared to the 50µM concentration. An unpaired T-test was performed.

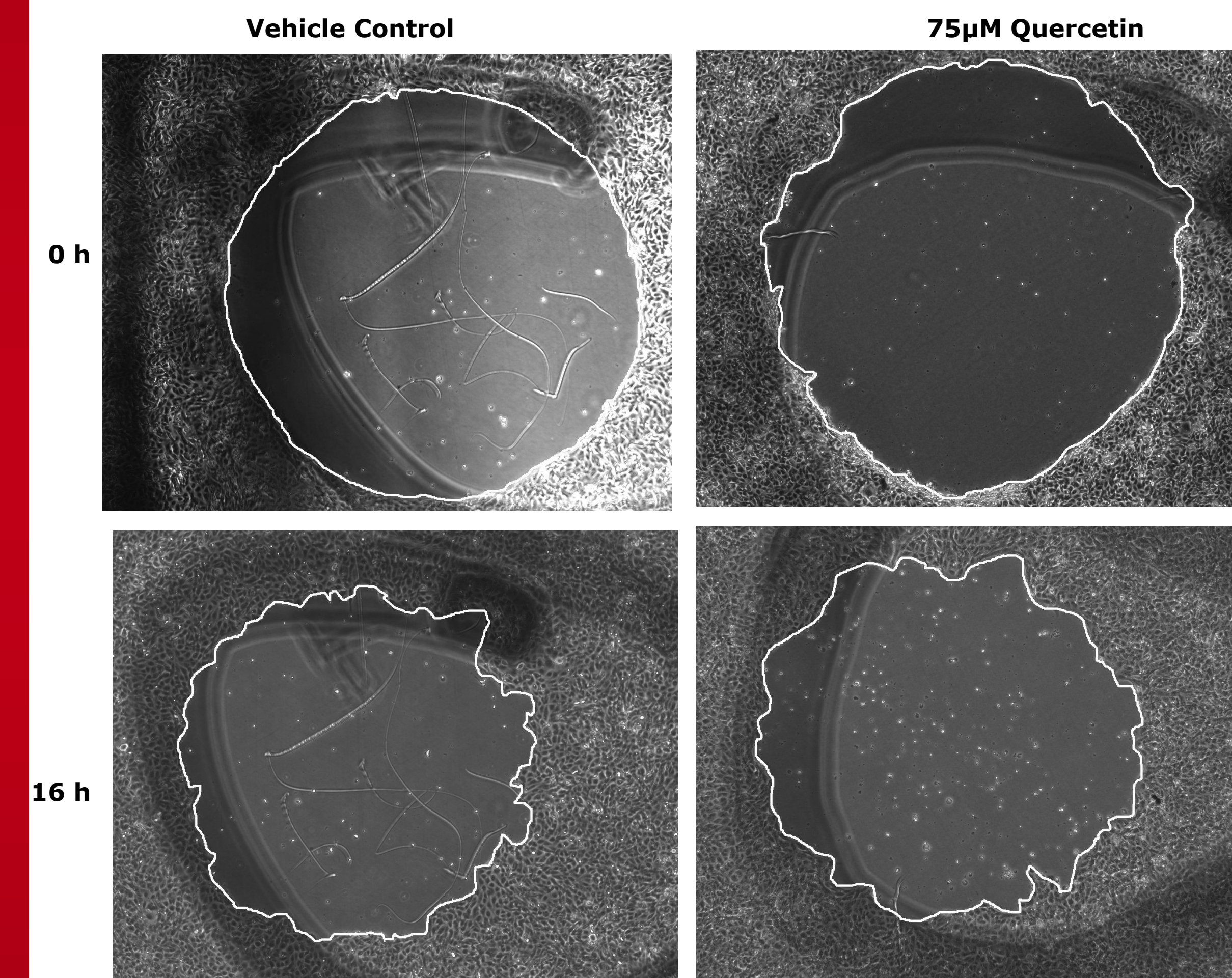


Figure 2. Quercetin inhibits the migration of E006AA prostate cancer cells. Cells were treated with quercetin (12.5-75µM). Cell migration assay was performed and photographed under phase-contrast microscopy (4x). Quercetin inhibits the migration of prostate cancer cells E006AA (P < 0.0001). Statistical significance was determined using the Kruskal Wallis Test, adjusted for multiple pairwise comparisons using the Dunn's test.

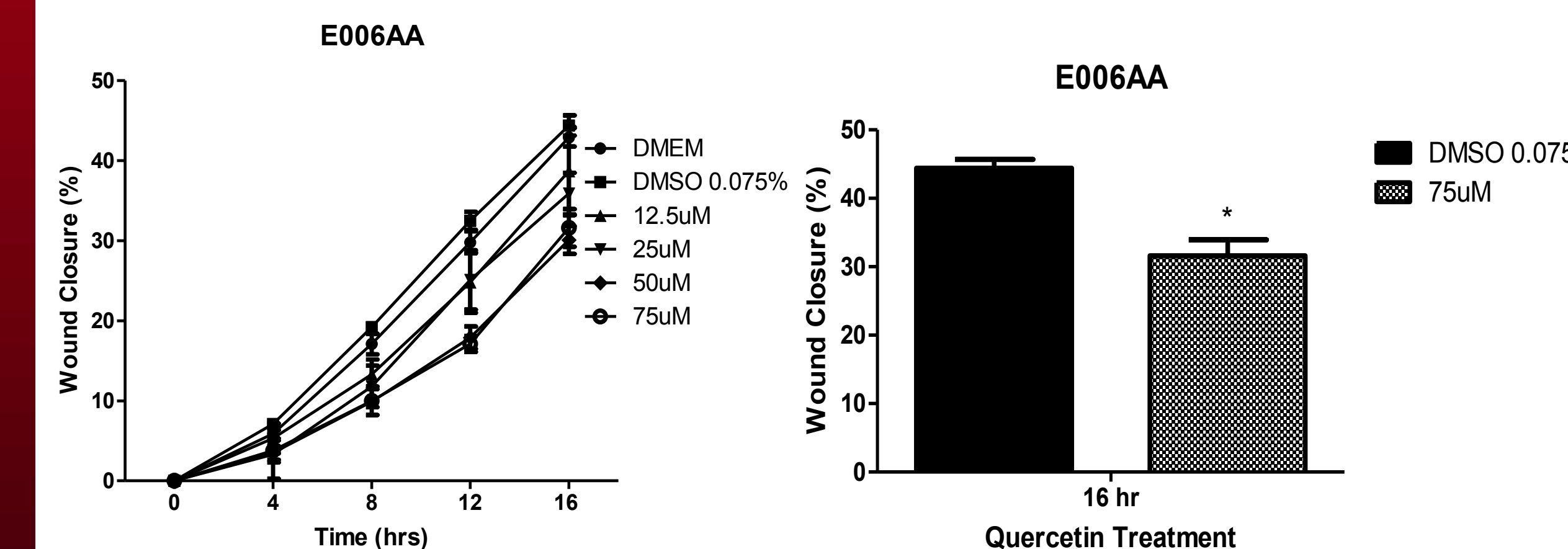


Figure 3. E006AA cells were treated with 12.5-75µM quercetin. Cell movement were captured at time 0, 4, 8, 12, 16 hours. After 12 hour incubation with quercetin (50µM and 75µM), cell migration decreased by 44.9%-47.4% with 50µM and 75µM of quercetin respectively, compared to vehicle control (DMSO 0.075%) (P<0.0001). Statistical significance level was based on a Kruskal Wallis Test, adjusted for multiple pairwise comparisons using the Dunn's test.

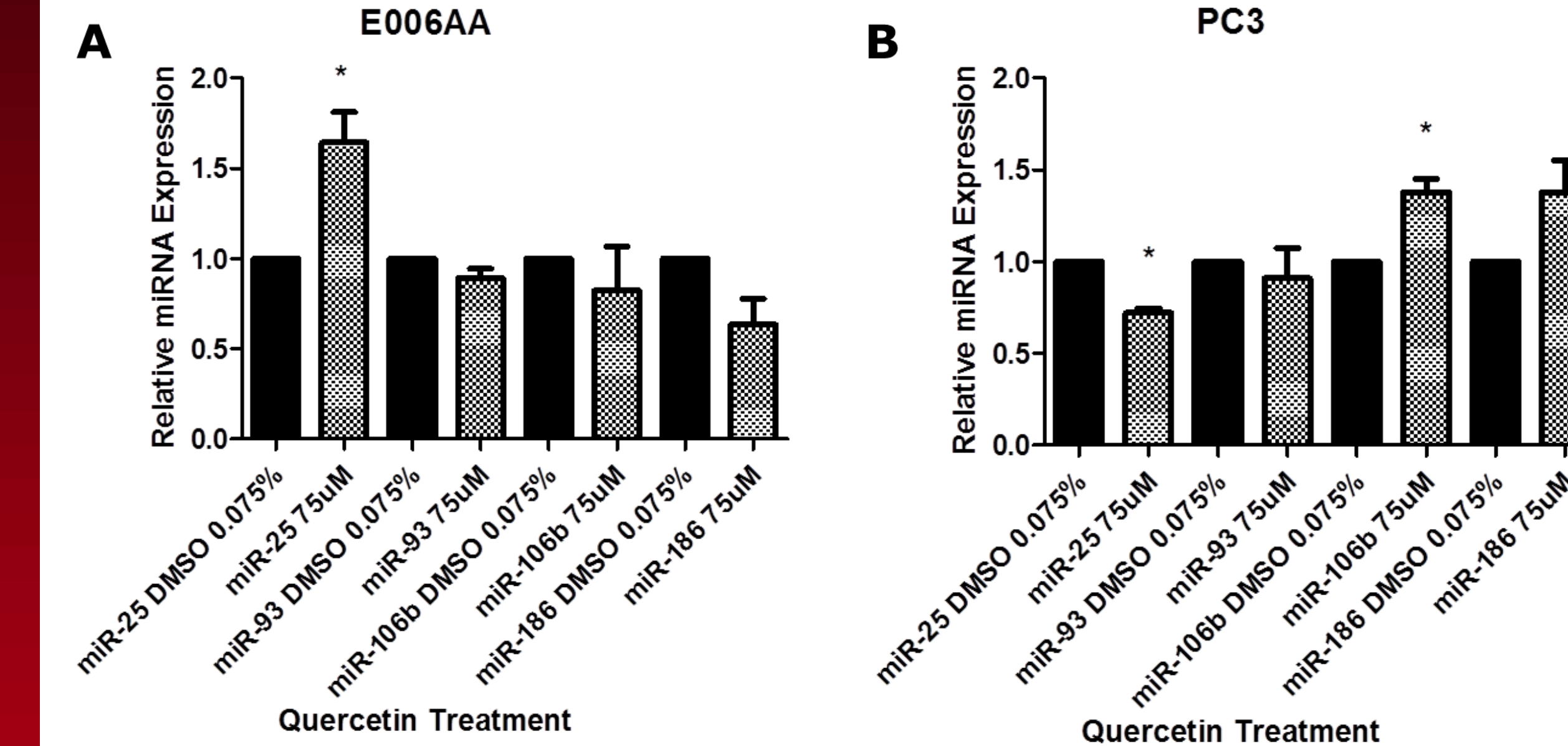


Figure 4. E006AA (A) and PC-3 (B) cells were treated with 75µM quercetin for 24 hours. Following quercetin treatment, miR-25 levels were increased by 64% in E006AA but decreased by 29% in PC3 cell lines. The expression of miR-106b was increased 38% in PC3 cell lines. Means±standard deviations are based on duplicates of two independent studies (P < 0.0001). Statistical significance level was based on a Kruskal Wallis Test, adjusted for multiple pairwise comparisons using the Dunn's test.

RESULTS

The study findings revealed that E006AA cells treated with quercetin (50-75µM) influences cell proliferation and migration.

We demonstrated a 39-97% increase in cell viability for the E006AA cells with 12.5-75µM quercetin treatment.

Quercetin treatment at 75µM revealed a 47.4% reduction in cell migration following a 16h incubation period using E006AA PCA cell lines

Quercetin (75µM) treatment up-regulated the expression of miR-25 by 64% in the E006AA cell lines; however, this miR was down-regulated by 29% in PC3 cell lines. up-regulated the expression of miR-106b by 38% in PC3 cell lines. Did not have significant effects on miRs -186 and -93.

DISCUSSION & FUTURE DIRECTIONS

Quercetin treatment significantly inhibited cell migration and up-regulated the expression of miR-25 in E006AA cell lines.

Relative to quercetin treatment at 50µM, we observed a significant (-72%) decrease in cell viability at the 75µM concentration.

Modify cell proliferation and cell migration assays using a wider quercetin dosage range (2.5µM-175µM) and lower %DMSO (i.e., 0.01%)

Determine whether quercetin treatments will: Down-regulate the expression of oncomiRs or up-regulate the expression of tumor suppressing miRs using next generation sequencing

Reduce aggressive PCA phenotypes (i.e., cell proliferation, colony formation, cell invasion) using metastatic PCA (i.e., LNCAP, DU145, MDA-PCA-2a, MDA-PCA-2b) and normal prostate epithelial (i.e. RWPE1, RWPE2) cell lines.

Reduce tumor size, tumor number, or metastasis using animal models

Modify miRNA targets and corresponding proteins using PCA or normal epithelial cell lines transfected with miRNA mimics or inhibitors

Evaluate whether a quercetin metabolite or quercetin analogs will have a more pronounced effect on modulating the expression of human miRs and/or PCA phenotype

Assess whether quercetin treatment combined with conventional/nutraceuticals may help increase survival rates among pre- or metastatic PCA patients

ACKNOWLEDGEMENTS

NCI R25 Cancer Education Grant to D.W. Hein (CA134283)

"Our Highest Potential" Endowed Chair in Cancer Research Endowment to LRK

Analysis of Mutant Epidermal Growth Factor Receptor Trafficking and Signaling in Lung Cancer Cells



Tejas N. Sangoi¹, Adriana S. Bankston², and Brian P. Ceresa²

¹R25 Cancer Education Program, University of Louisville

²Department of Pharmacology and Toxicology, University of Louisville

Abstract

Purpose: To better understand how activating mutants of epidermal growth factor receptor (EGFR) regulate trafficking and signaling of the receptor in lung carcinoma cells.

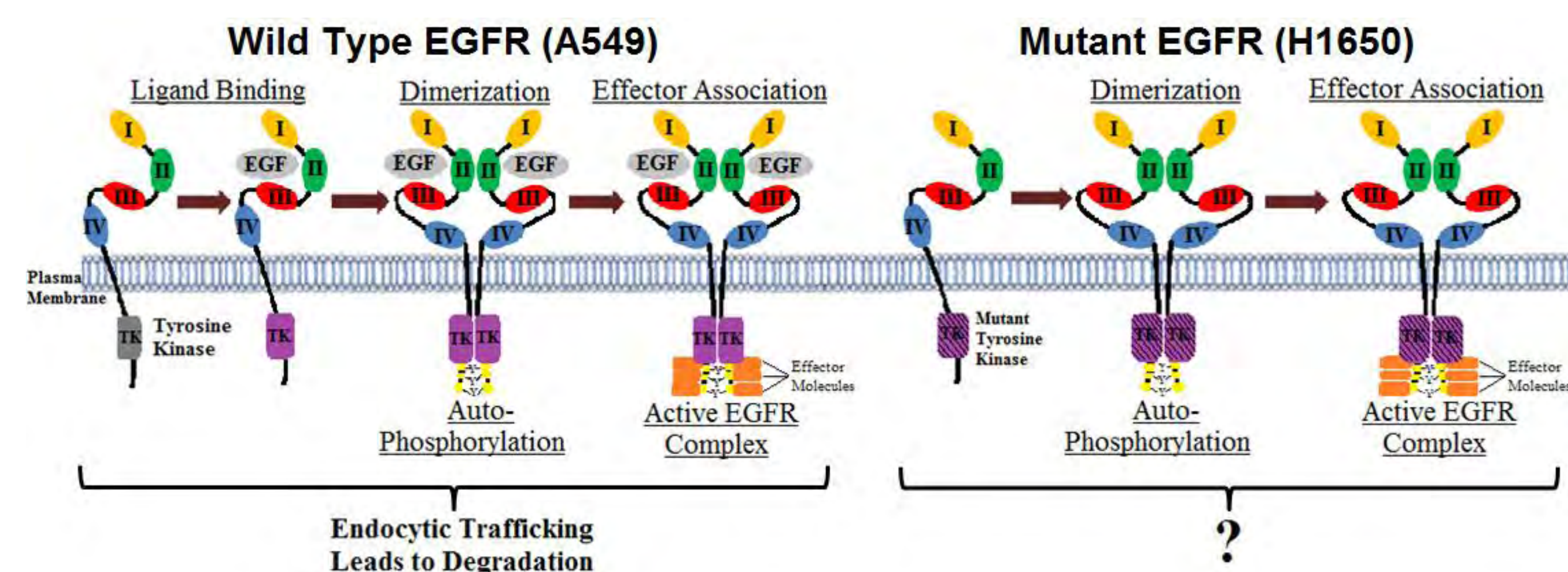
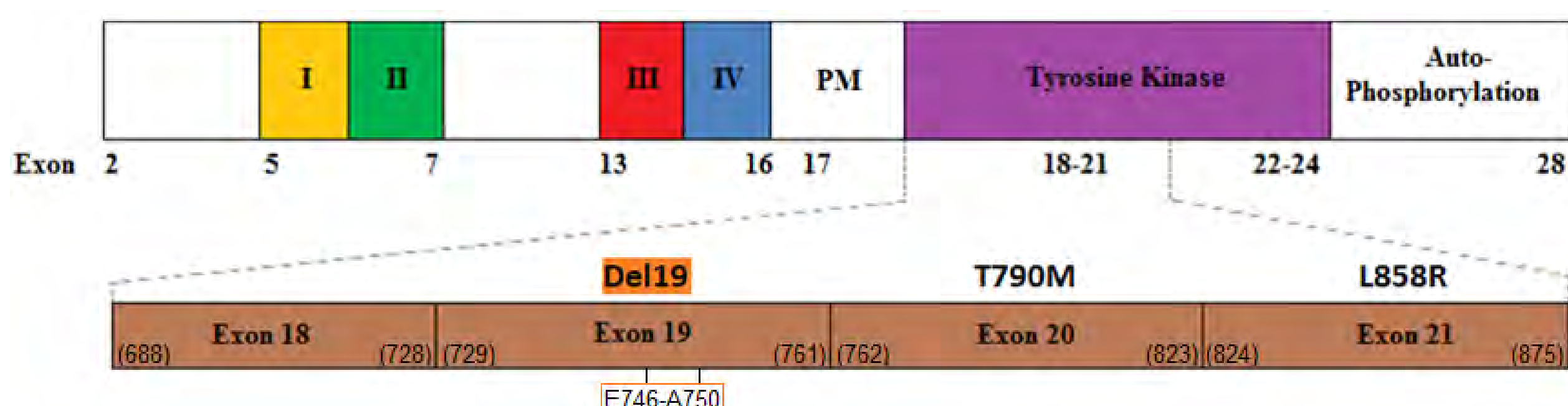
Methods: H1650 cells express mutant EGFRs; A549 cells express wild type EGFRs. Immunoblotting was used to test for time-dependent EGFR phosphorylation and degradation upon EGF stimulation. Receptor trafficking and endosomal accumulation at steady state were observed by immunofluorescence staining of the total EGFR. The pattern of EGFR constitutive recycling of the receptor was examined by incubating with Ab1 antibody. Kinetics of ¹²⁵I-EGF endocytosis and ligand-mediated degradation were measured by radioligand binding assay.

Results: Immunoblotting for phosphorylated EGFR shows an increase in steady state EGFR phosphorylation, as well as elevated phosphorylation of effector molecules MAPK and MEK in H1650 cells. Steady state distribution of unliganded, mutant EGFR through immunostaining indicates localization in the early endosome. After 24 hours of Ab1 treatment, mutant EGFRs show increased endosomal accumulation. Furthermore, mutant EGFRs exhibit a slower rate of recycling and degradation.

Conclusions: Activating mutants of EGFRs found in lung cancer cells have higher levels of phosphorylation in EGFR Y1068, MAPK, and MEK. Localization of mutant EGFR is seen in the early endosome at steady state, as well as a defect in constitutive membrane trafficking after 24 hours. Less radioligand recycling and degradation in the mutant lung cancer cell lines indicate a defect in endocytic trafficking.

Introduction

- Lung cancer is a major health concern in the Commonwealth of Kentucky, and there are more deaths in the U.S. from lung cancer than any other cancer. (www.cdc.gov)
- Specifically, over 85% of lung cancers are non-small cell lung cancer (NSCLC), and cells from NSCLC patients are used in this project. (www.cancer.org)
- Many NSCLC cells are characterized by activating EGFR mutations.
- EGFR is a receptor tyrosine kinase that is normally activated by ligand binding, and inactivated by either endocytic recycling or degradation.
- Mutant EGFR have constitutive kinase activity, which modulate downstream signaling in the absence of ligand.
- Del19 mutations are in-frame deletions at exon 19 (E746-A750) that occur in 48% of all EGFR mutant NSCLC cells; although patients are responsive to EGFR tyrosine kinase inhibitor therapies, many become resistant over time. (www.mycancergenome.org)



In its unstimulated state, the wild type EGFR is a monomer on the cell surface. Upon ligand binding, the receptor undergoes a conformational change which leads to receptor dimerization and activation of the intracellular kinase domain (purple box). Receptor pairs trans-phosphorylate, yielding C-terminal phosphotyrosine; these phosphotyrosines serve as docking sites for downstream signaling proteins. In contrast, mutant EGFRs have constitutive kinase activity, and thus proceed with the dimerization, auto-phosphorylation, and effector association steps without a ligand present.

Hypothesis: Del19 mutant epidermal growth factor receptors have altered endosomal trafficking and signaling in lung cancer cells.

Figure 1

Elevated EGFR Y1068, MapK, and Mek phosphorylation in mutant lung cancer cells

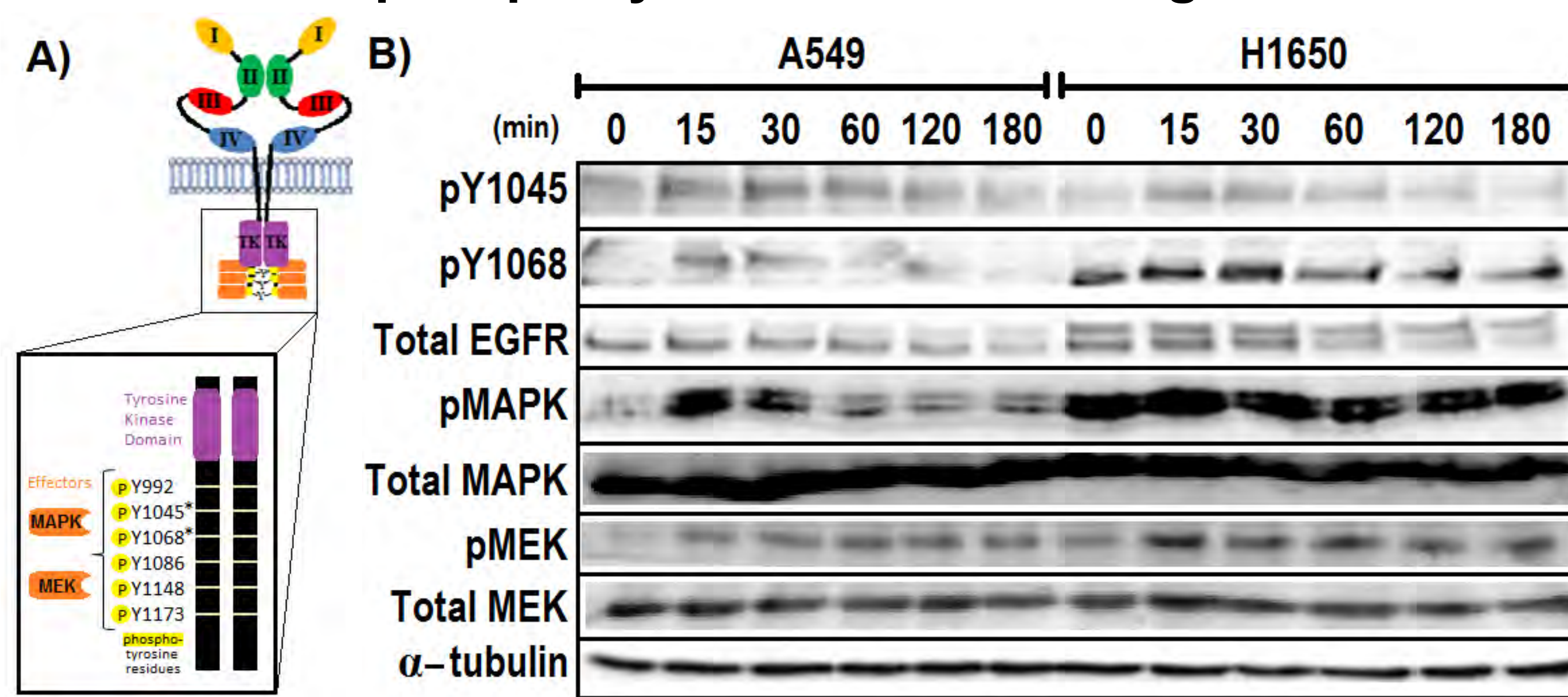


Figure 1. A) Schematic of the EGFR, with a close-up of the intracellular domain. B) A549 & H1650 cells were serum starved and treated for 0-180 minutes with 10 ng/mL of EGF. Cell lysates were harvested and equivalent amounts of protein were resolved through SDS-PAGE. Gels were transferred to nitrocellulose and probed for various proteins. Phosphorylation of EGFR at Y1045 is unchanged, whereas at Y1068 it is elevated in H1650 cells. The effector proteins MAPK and MEK also exhibit elevated phosphorylation in H1650 cells. The total EGFR, MAPK, and MEK remain relatively unchanged. α -tubulin is used as a loading control. The results shown are representative blots from an experiment performed n=3-5 times.

Figure 2

Mutant EGFRs localize in the early endosome at steady state

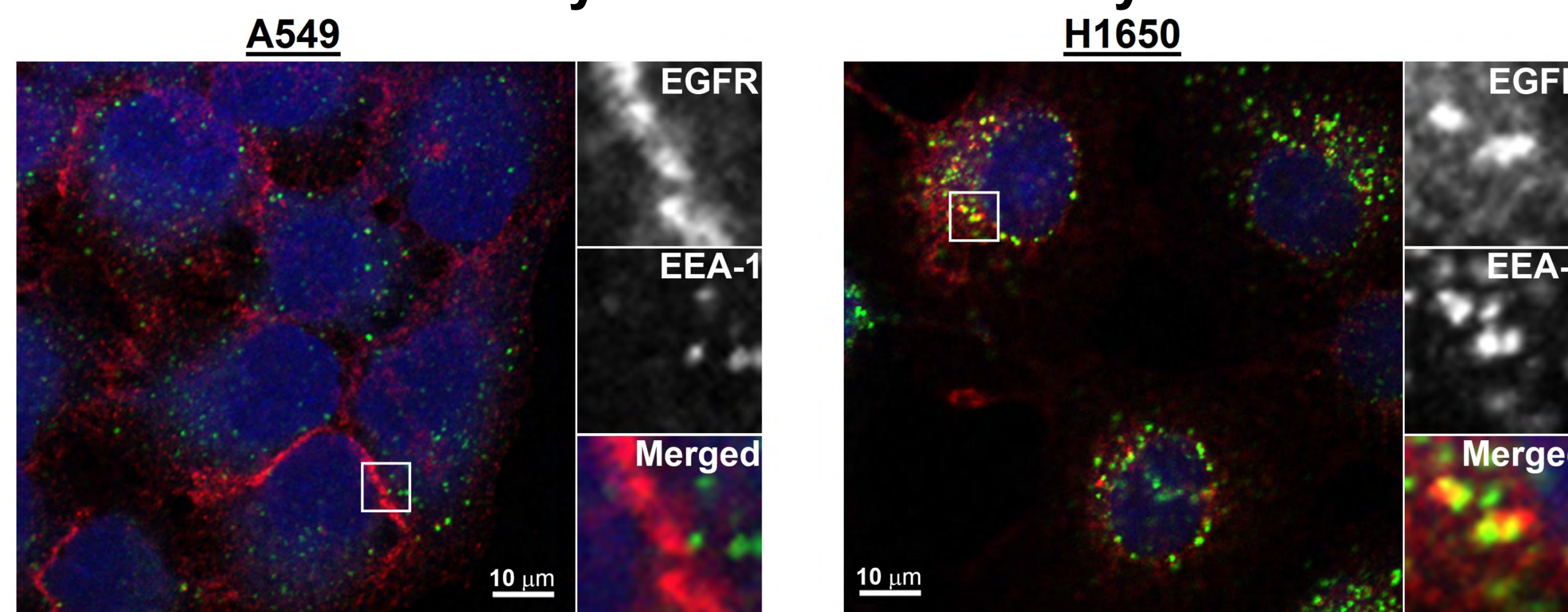


Figure 2. A549 & H1650 cells were grown on coverslips until they were 90% confluent. Cells were fixed, permeabilized, and stained for EGFR (Ab1), EEA-1 (early endosomal marker), and DAPI. Z-stack images were collected with a confocal microscope; only slices at the center of the cells are shown. Scale bar = 10 μ m.

Figure 3

Mutant EGFRs show a defect in constitutive membrane

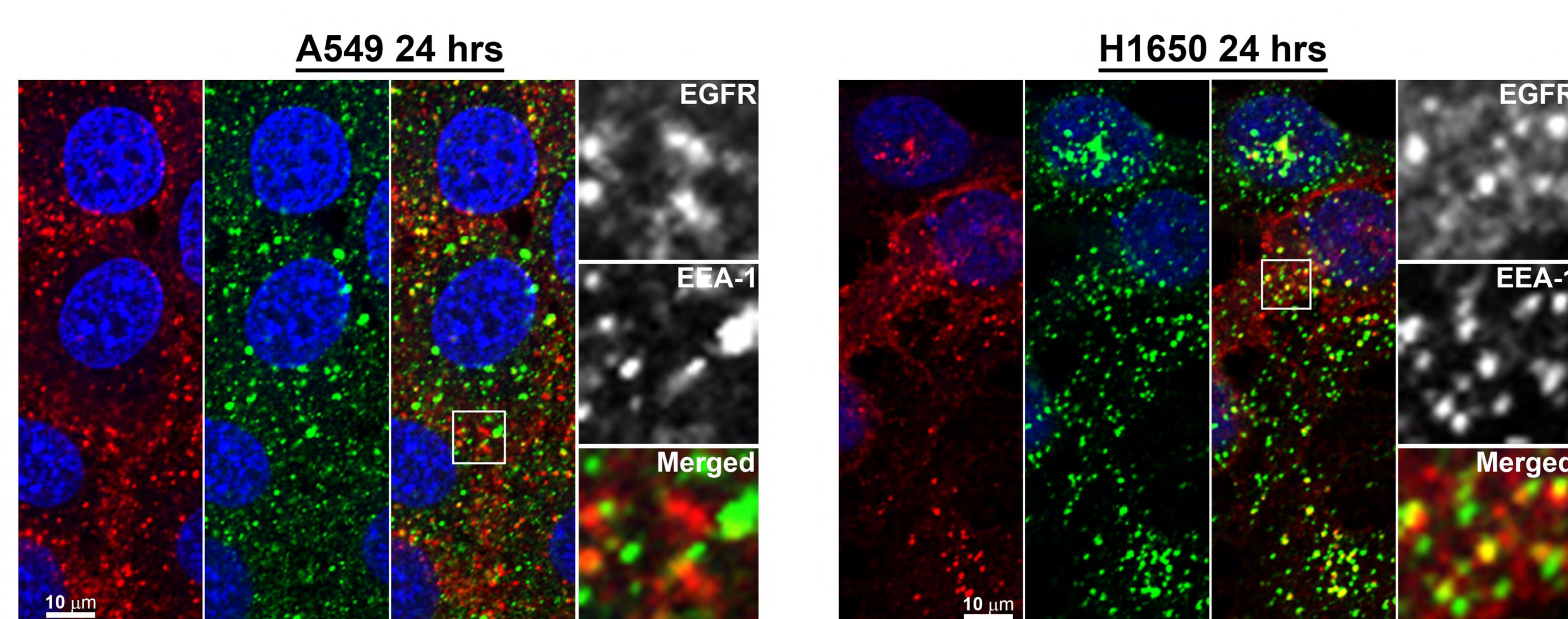


Figure 3. A549 & H1650 cells were grown on coverslips until they were 90% confluent. Cells were treated with 1 μ g/mL Ab1 (EGFR antibody) for 24 hours. Cells were fixed, permeabilized, and stained for EGFR (Ab1), EEA-1 (early endosomal marker), and DAPI. Z-stack images were collected with a confocal microscope; only slices at the center of the cells are shown. Scale bar = 10 μ m.

Figure 4

Mutant cells show less secretion and degradation in ¹²⁵I-EGF binding assay

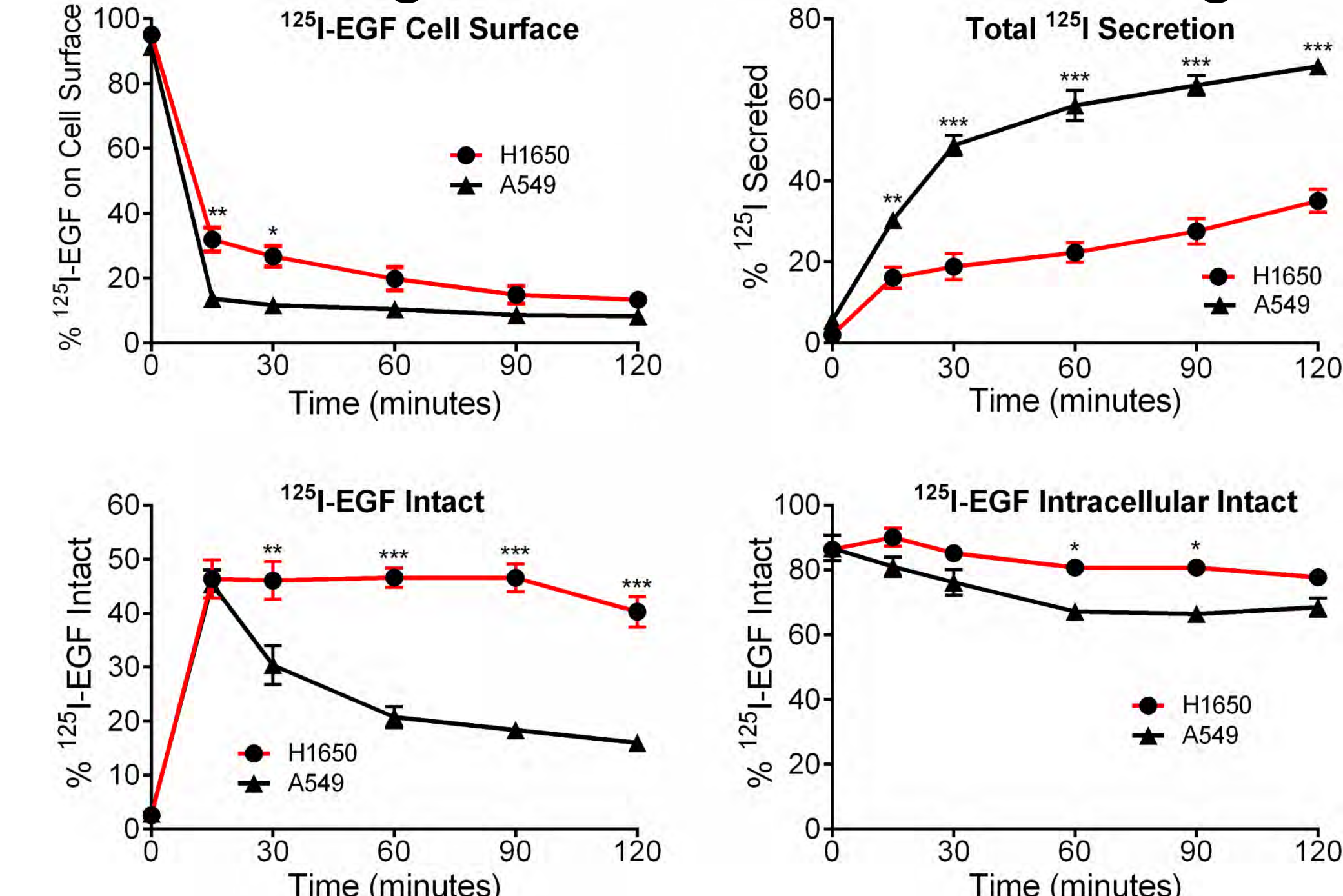


Figure 4. A549 & H1650 cells were incubated on ice with 0.05 μ g/mL ¹²⁵I-EGF until steady-state cell surface binding was achieved. Free radioligand was removed and cells were placed at 37°C. At each time point, samples were collected to determine the total secreted, cell surface, intact, and intracellular ¹²⁵I-EGF. Intracellular ¹²⁵I-EGF was TCA precipitated to determine the amount of degraded and intact ¹²⁵I-EGF. The data shown are average \pm S.E.M. H1650, n=5; A549, n=3.

Figure 5

Model of Del19 EGFR endocytic trafficking

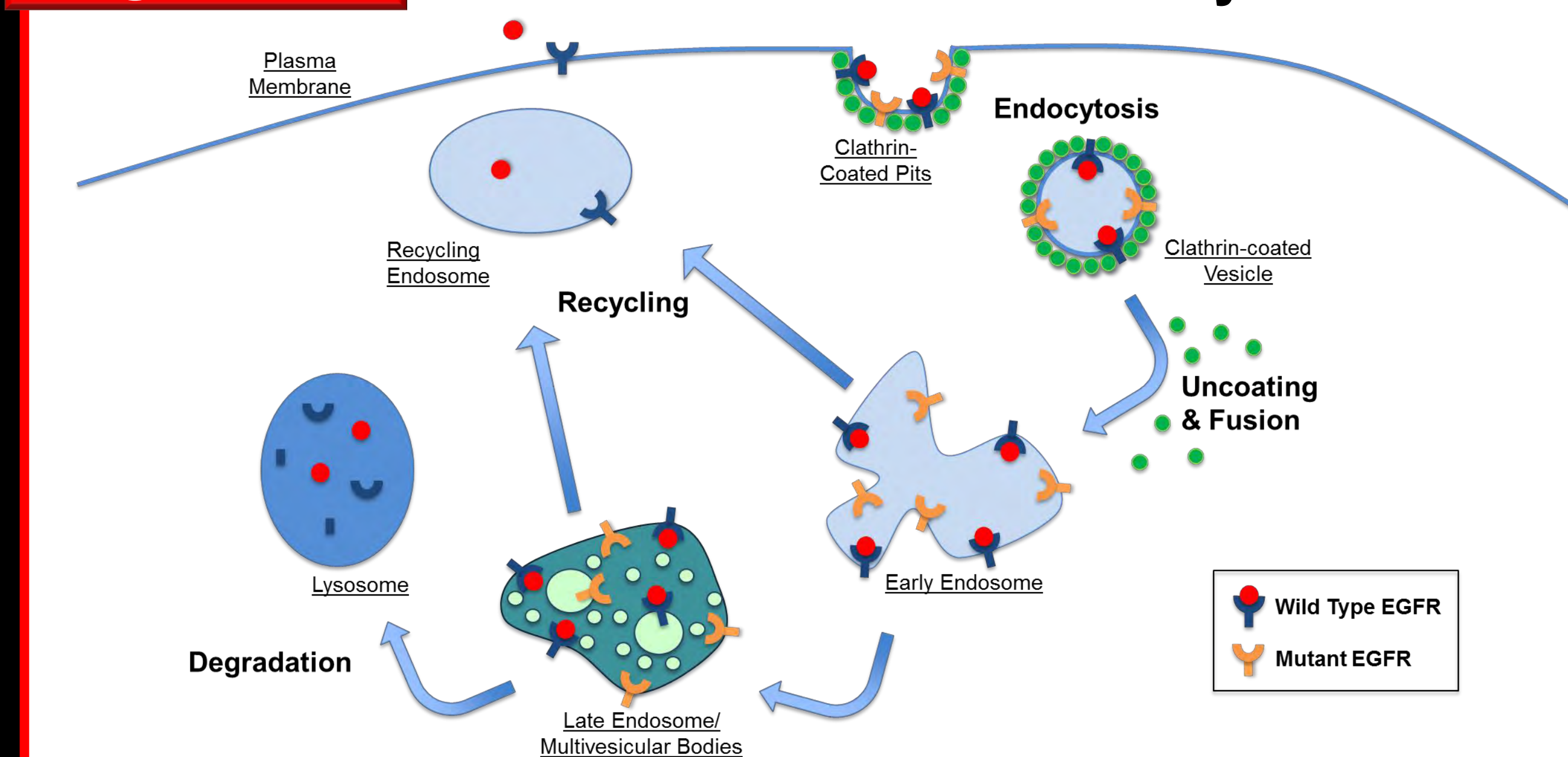


Figure 5. Both wild type and Del19 mutant EGFRs enter the cell via clathrin-coated pits. The EGFR is contained in the resulting clathrin-coated vesicles, which shed its clathrin and fuse with an early endosome. Wild type EGFR then gets sorted to either be recycled to the plasma membrane or degraded via the lysosome. Mutant EGFRs appear to have less recycling and degradation, and seem to accumulate in the endosome.

Conclusions

- Lung cancer cells with activating mutants of EGFRs exhibit:
- Elevated phosphorylation on EGFR Y1068 and effectors MAPK and MEK.
 - Localization of mutant EGFR at steady state in the early endosome.
 - A defect in constitutive membrane trafficking after 24 hours.
 - Less radioligand recycling and degradation

Overall Conclusion: Endosomal accumulation indicates a defect in the endocytic trafficking of del19 mutant EGFRs.

Future Experiments: determine if del19 mutants are localizing in other compartments; investigate phosphorylation of other effector molecules downstream of constitutively activated EGFRs.

Acknowledgements

R25 Cancer Education Program, Ceresa Lab Members
Funding: NCI R25-CA134283, NIH R01-GM092874.

Effects of Nanoparticle Morphology and Surface Modification on Tumor Penetration and Distribution

Lee B. Sims¹, Hermann Frieboes¹, Jill M. Steinbach¹

Department of Bioengineering¹

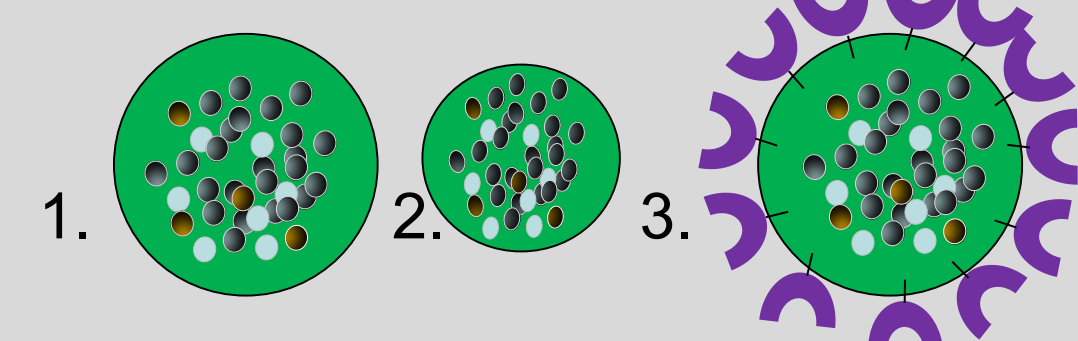
University of Louisville J. B. Speed School of Engineering

Introduction

One of the challenges to efficacious drug and gene delivery to solid tumors is inadequate penetration and distribution throughout the tumor vasculature. To overcome these challenges, nanotechnologies such as nanoparticles (NPs), can be utilized to protect agents during delivery, prolong delivery, and safely localize drugs and biologics to the tumor microenvironment. In addition to these attributes, NPs can be modified to enhance penetration and distribution throughout the tumor vasculature. Different factors including: NP surface charge, surface composition, size, and shape are integral to enabling drug delivery vehicles to withstand systemic interactions and to transport to the tumor site. The long-term goal of this study is to develop adaptable poly(lactic-co-glycolic acid) PLGA NPs with a variety of surface modifications and sizes to evaluate how each modification contributes to 3-D distribution in a tumor spheroid model. In combination with mathematical modeling to predict formulations that will enhance distribution, experimental validation will enable us to rationally design NP formulations that successfully penetrate the tumor microenvironment. We hypothesize that ultra-small (< 70nm) and/or surface-modified NPs will improve targeting of, and penetration to the tumor spheroid, and will significantly enhance NP uptake to individual cells. The experiments conducted here provide us with a preliminary assessment of design factors governing NP-tumor interactions in a 3-D environment. We expect these and future experiments will provide insight to select efficacious modifications for increased tumor targeting and distribution.

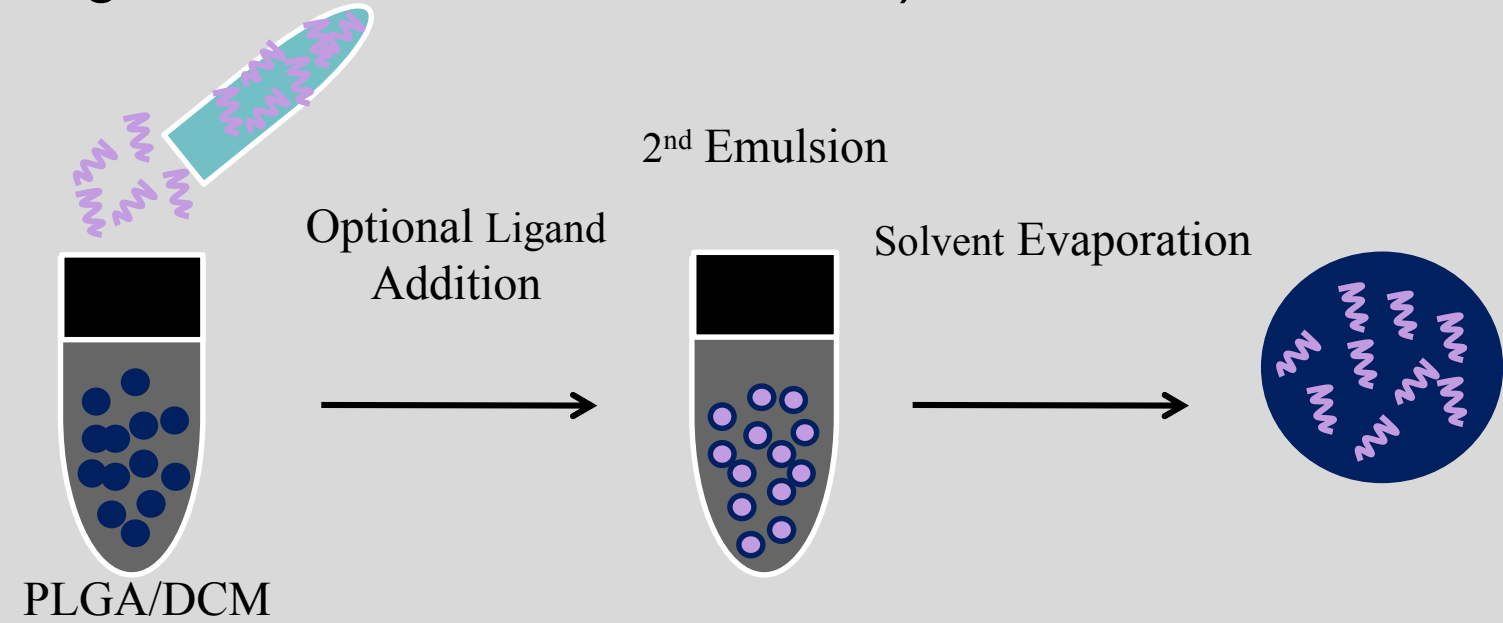
Methods

In this study, we synthesized and characterized PLGA NPs encapsulating a fluorescent dye, Coumarin 6 (C6), to evaluate tumor penetration and distribution via fluorescent microscopy. To initiate our studies, three different NP formulations were synthesized: 1) PLGA unmodified, 2) PLGA ultra-small unmodified, 3) PLGA surface-modified NPs.



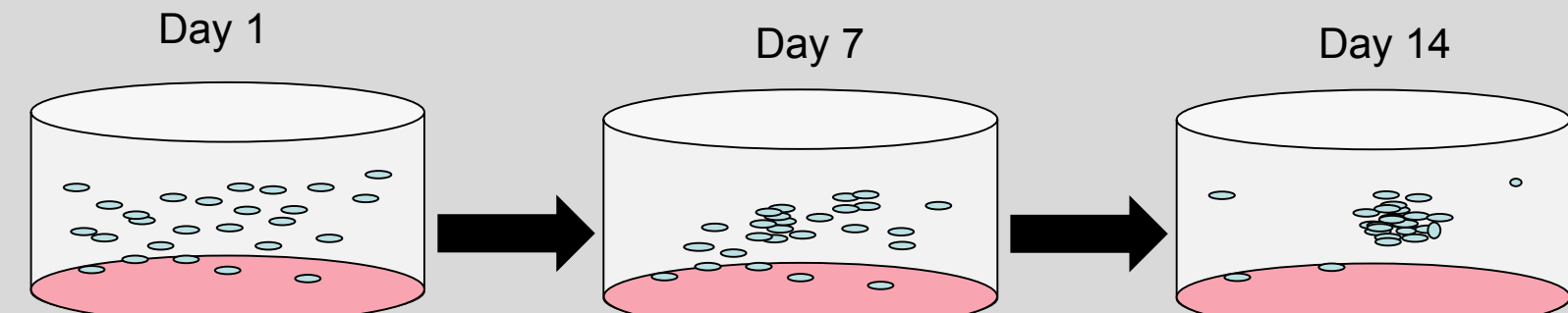
Nanoparticle Fabrication

C6 NPs were synthesized using an oil-in-water single emulsion technique. For surface-modified NPs, avidin-palmitate was conjugated to the NP surfaces for subsequent reaction with biotinylated ligands (PEG, CPPs). For ultra-small NPs, supernatant after the first centrifugation was saved and further centrifuged to obtain sub-70nm NPs.



Tumor Spheroid Formation

HeLa cervical cancer cells were used to form tumor spheroids, which closely mimic the human tumor physiological environment *in vitro*. Tumor spheroid cultures were formed using the liquid overlay method. This method inhibits the attachment of cells to tissue culture plates and promotes cell-cell aggregation. Prior to spheroid formation, 24-well tissue culture plates were coated with a 1% (w/v) agarose gel to prevent cells adhering to the plate. Cells were subsequently added to each well and lightly shaken for 15 minutes. NP distribution experiments followed after incubation at 37°C for 14 days.



To visualize NP distribution within the tumor spheroid, a 1mg/ml solution of ultra-small and regular NPs were incubated with the spheroids at three different time points: t=1hr, 6hr, and 24hr. After incubation, spheroids were washed with PBS and then transferred to a MatTek 14mm glass bottom imaging dish. For these experiments, we utilized both confocal microscopy and inverted epifluorescent microscopy.

Results: Nanoparticle Characterization

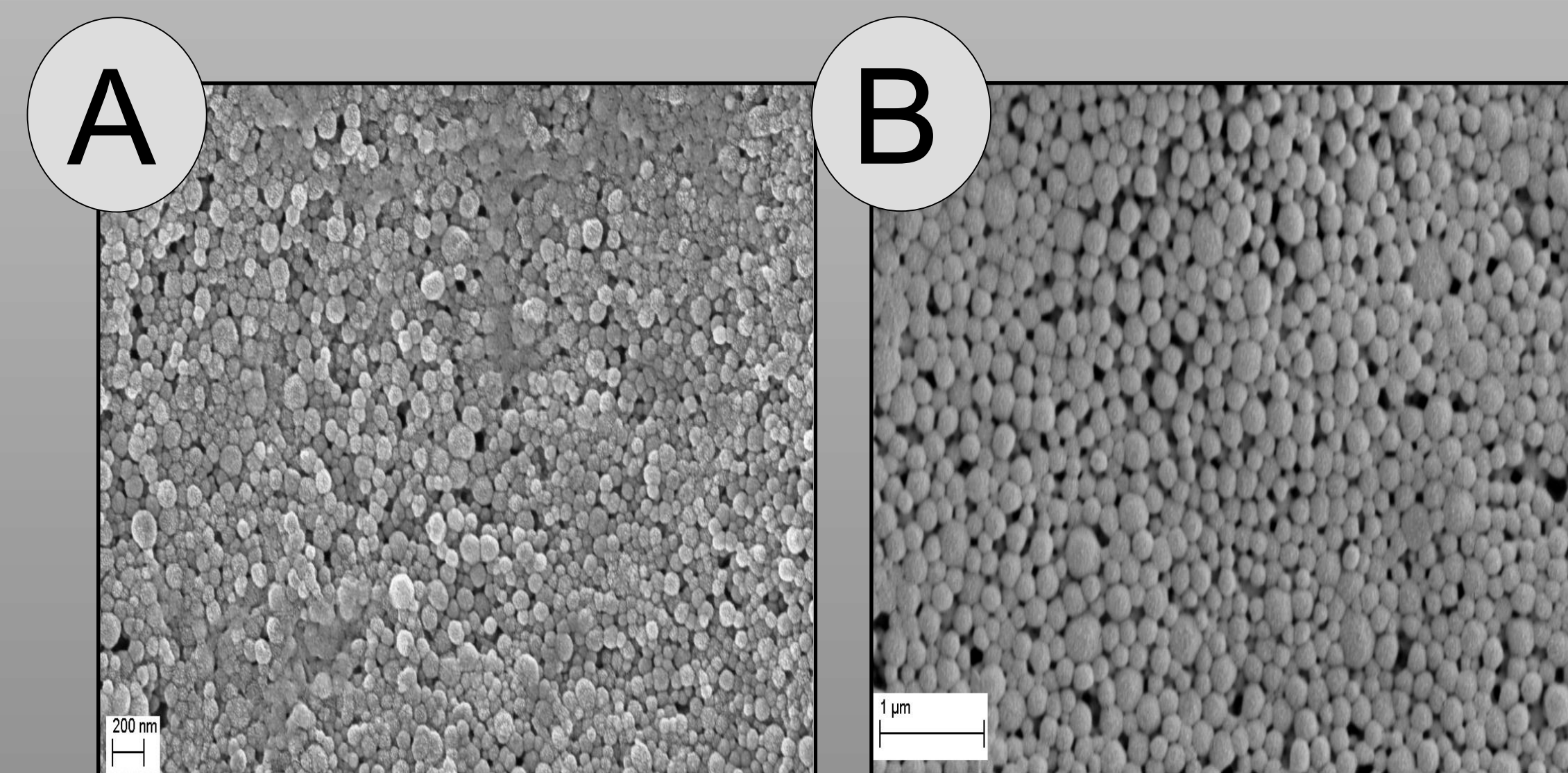


Figure 1: Scanning electron microscope (SEM) images of: (A) ultra-small C6 NPs and (B) regular C6 NPs.

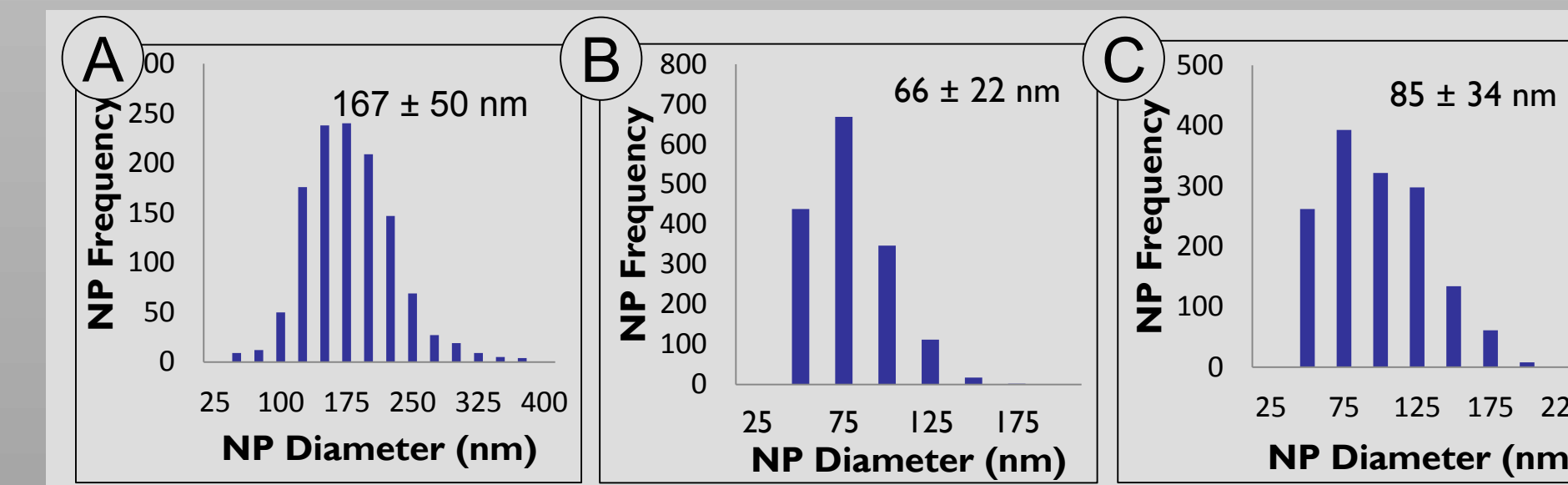


Figure 2: Nanoparticle Sizing via SEM: (A) regular C6 NPs, (B) ultra-small C6 NPs and (C) PEG-modified NPs.

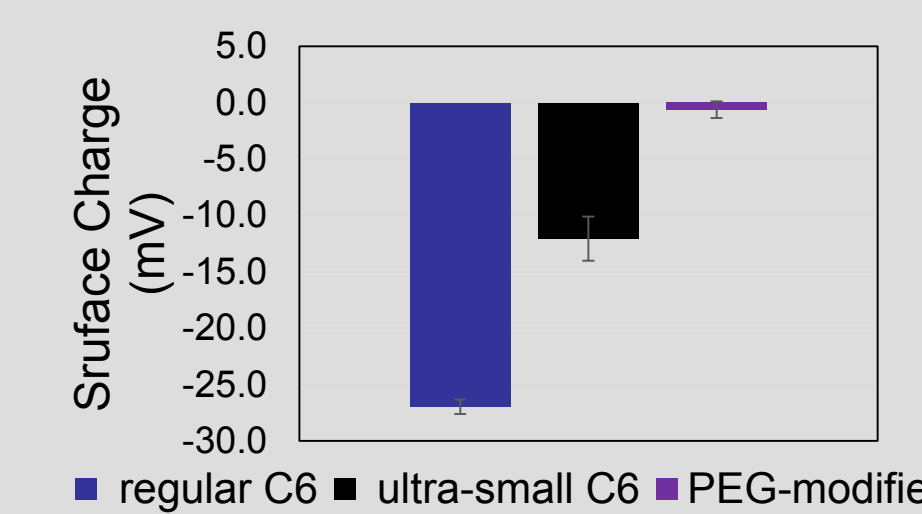


Figure 3: Nanoparticle surface charge.

Results: Spheroid Imaging

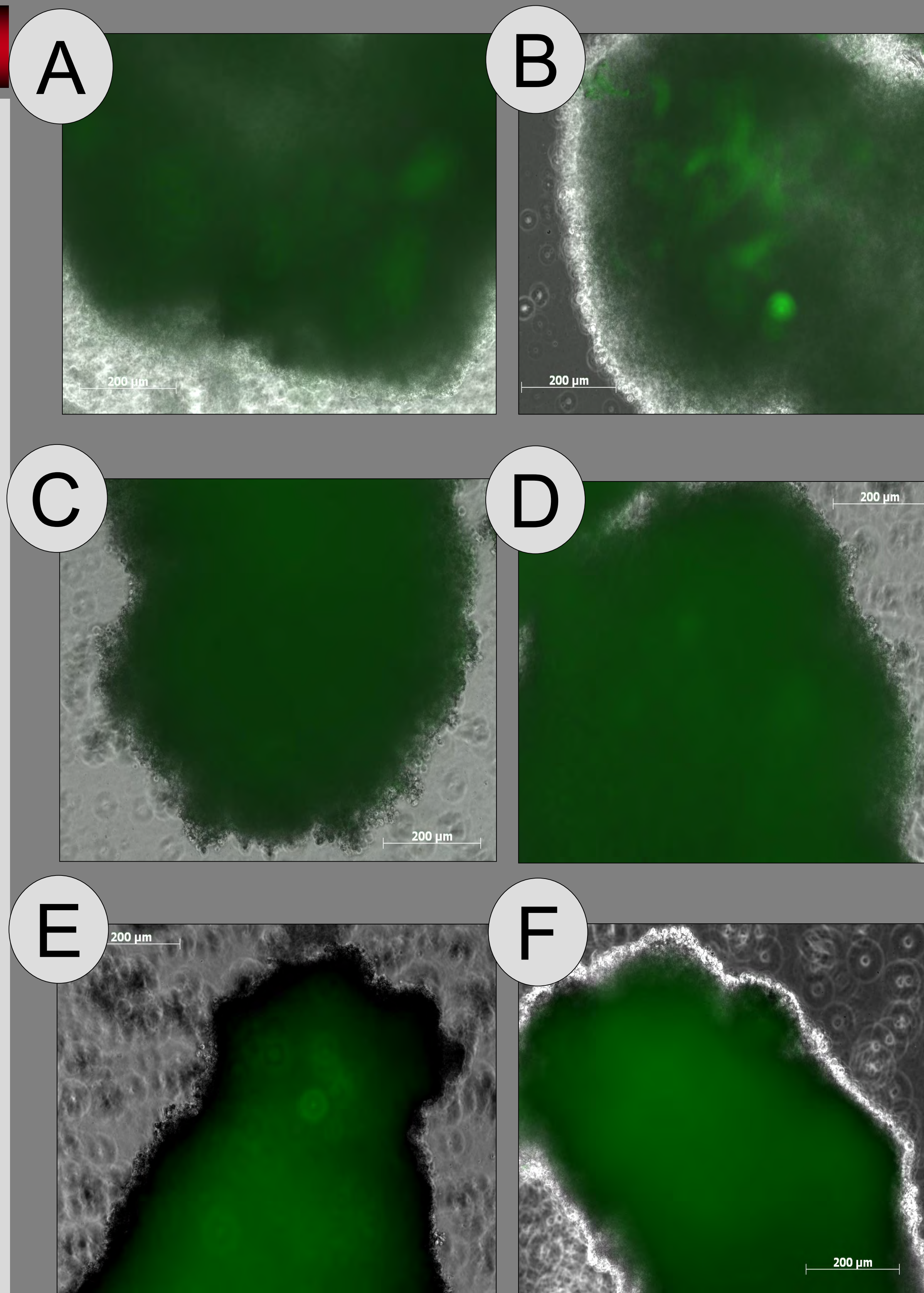


Figure 4: Tumor spheroid imaging using inverted epifluorescent microscopy for regular (A, C, E) and ultra-small (B, D, F) NPs. Images after 1hr. (A, B); 6hr. (C, D); and 24hr. (E, F) incubation times.

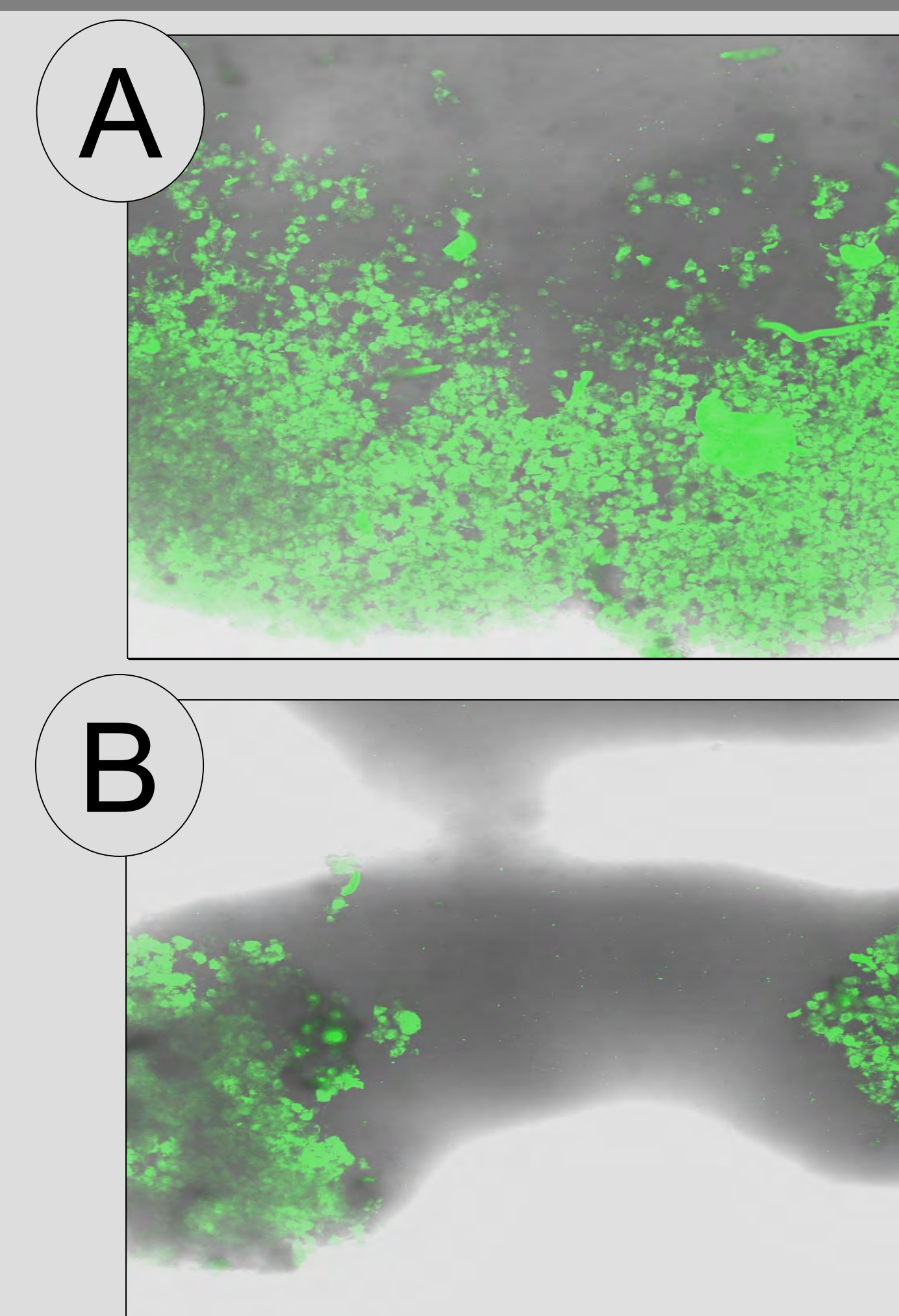


Figure 5: Tumor spheroid imaging using confocal microscopy for (A) ultra-small C6 NPs and (B) regular C6 NPs at 24hr.

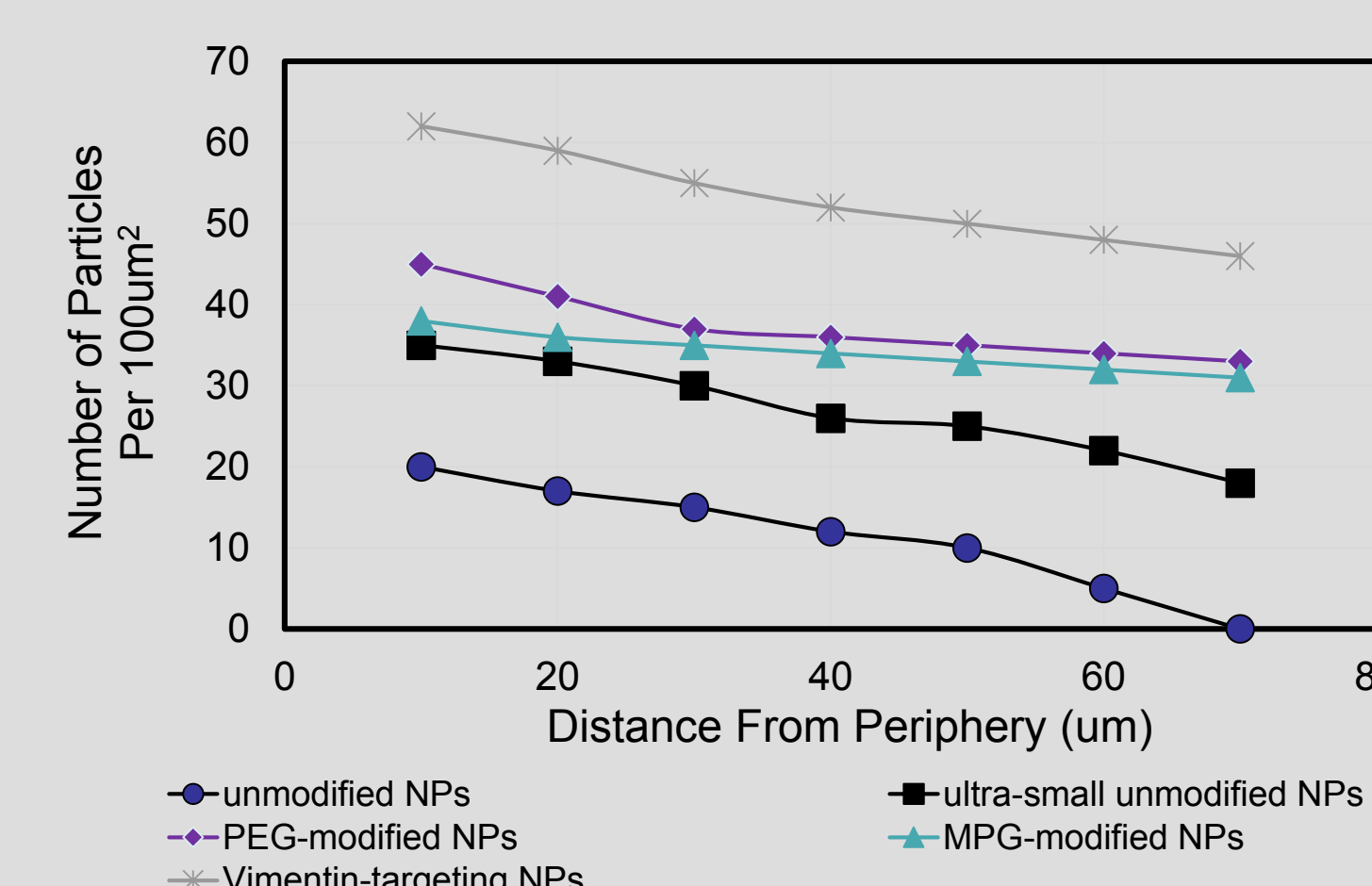


Figure 6: Expected NP distribution with respect to tumor periphery.

Future Studies

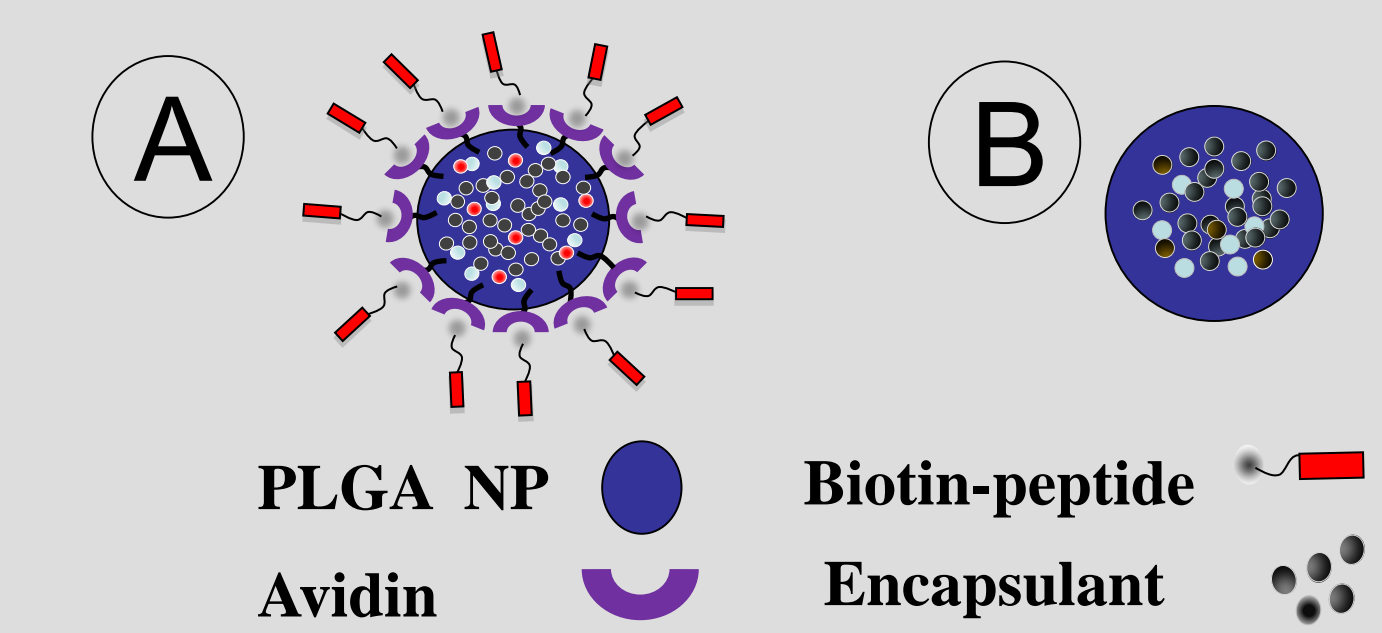


Figure 6: NP Schematic: (A) surface-modified and (B) unmodified NPs.

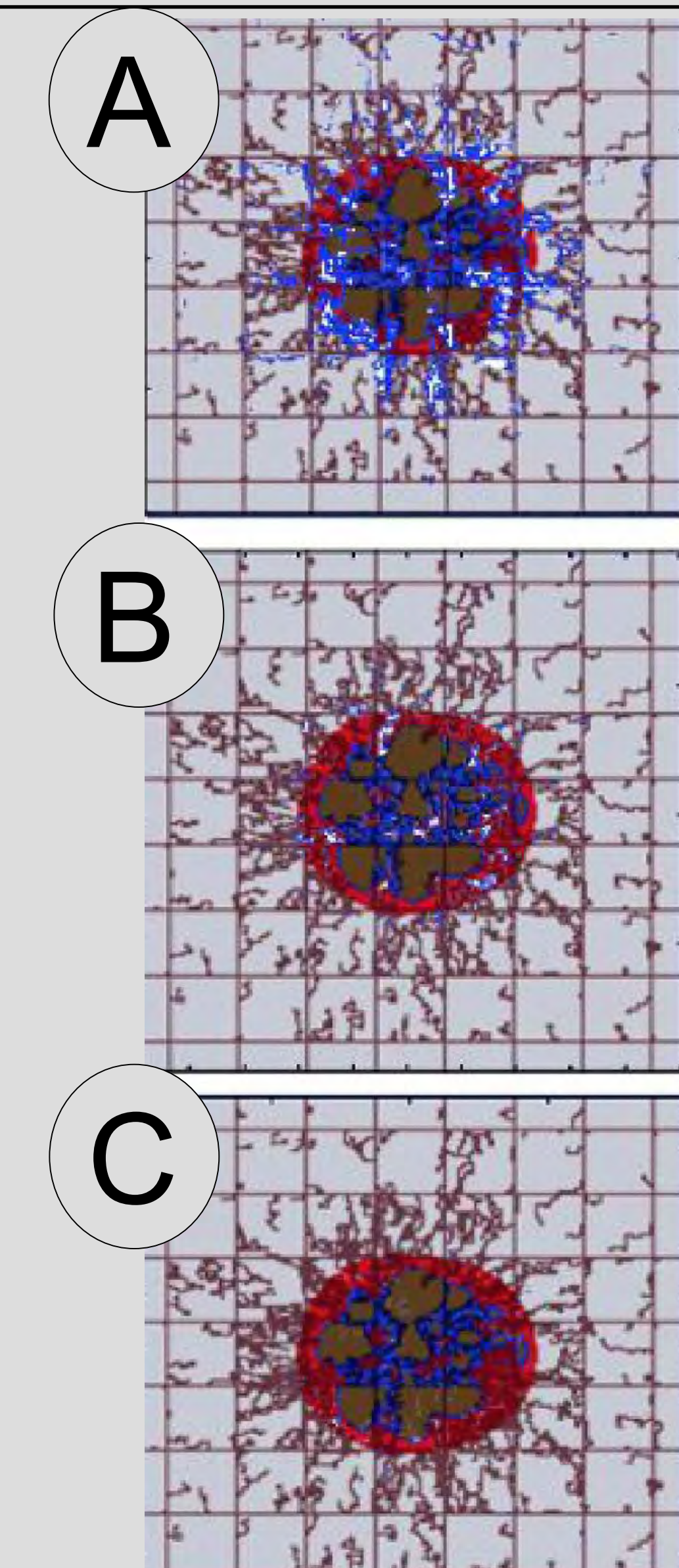


Figure 8: Expected NP distribution from computational math model of: (A) Vimentin-targeted (CPP+homing) NPs, (B) PEG-modified NPs and (C) ultra-small NPs.

Conclusions

- At time t=6hr, NPs become more dispersed and less punctate than t=1hr.
- Spheroids are saturated at a NP concentration of 1mg/ml. Lower concentrations (doses) may achieve successful penetration.
- Ultra-small NPs are able to penetrate the spheroid more efficiently than regular NPs.
- PEG-modified NPs are expected to navigate the tumor microenvironment and penetrate the tumor vasculature more efficiently than both ultra-small and regular NPs.
- NPs modified with a cell penetrating peptide are hypothesized to provide better penetration and uptake to tumor vasculature and individual tumor cells.
- Vimentin-targeting NPs (tumor homing + CPP) are postulated to target, penetrate, and distribute throughout the tumor model.

Acknowledgements

Research is supported by the University of Louisville Cancer Education Program NIH/NCI R25-CA134283.